2009-12

Combined integral and robust control of the segmented mirror telescope

Looysen, Michael W.

Monterey, California. Naval Postgraduate School

NAVAL POSTGRADUATE SCHOOL

MONTEREY, CALIFORNIA

THESIS

COMBINED INTEGRAL AND ROBUST CONTROL OF THE SEGMENTED MIRROR TELESCOPE

by

Michael W. Looysen

December 2009

Thesis Advisor:	Brij Agrawal
Co-Advisor:	Jae Jun Kim

Approved for public release; distribution is unlimited

THIS PAGE INTENTIONALLY LEFT BLANK

REPORT DOCUMENTATION PAGE			Form Approved OMB No. 0704-0188
Public reporting burden for this collection of information is estimated to average 1 hour per response, including the time for reviewing instruction, searching existing data sources, gathering and maintaining the data needed, and completing and reviewing the collection of information. Send comments regarding this burden estimate or any other aspect of this collection of information, including suggestions for reducing this burden, to Washington headquarters Services, Directorate for Information Operations and Reports, 1215 Jefferson Davis Highway, Suite 1204, Arlington, VA 22202-4302, and to the Office of Management and Budget, Paperwork Reduction Project (0704-0188) Washington DC 20503.			
1. AGENCY USE ONLY ***(Leave blank)***	**2. REPORT DATE** December 2009	**3. REPORT TYPE AND DATES COVERED** Master's Thesis	
4. TITLE AND SUBTITLE: Combined Integral and Robust Control of the Segmented Mirror Telescope		**5. FUNDING NUMBERS**	
6. AUTHOR(S) Michael W. Looysen			
7. PERFORMING ORGANIZATION NAME(S) AND ADDRESS(ES) Naval Postgraduate School Monterey, CA 93943-5000		**8. PERFORMING ORGANIZATION REPORT NUMBER**	
9. SPONSORING /MONITORING AGENCY NAME(S) AND ADDRESS(ES) N/A		**10. SPONSORING/MONITORING AGENCY REPORT NUMBER**	
11. SUPPLEMENTARY NOTES The views expressed in this thesis are those of the author and do not reflect the official policy or position of the Department of Defense or the U.S. Government.			
12a. DISTRIBUTION / AVAILABILITY STATEMENT Approved for public release; distribution is unlimited		**12b. DISTRIBUTION CODE**	

13. ABSTRACT (maximum 200 words)

Future space telescopes must maintain lower mass of the mirrors to keep launch cost down while increasing the size and performance of the space telescope. Although much work has been done in both adaptive optics and robust control, this thesis explores the application of several Multi-Input, Multi-Output controller designs for wavefront control of a Segmented Mirror Telescope with 936 actuators and 732 sensors. This thesis builds on previous robust control design by combining classical control with an H_∞ robust controller on a Singular Value Decomposition reduced model. It also presents reduction using Zernike polynomials and applies it to the integral control model as an alternate to Singular Value Decomposition model reduction.

All methods were able to meet the 10 Hz bandwidth by design. Therefore, the analysis shows that there are several trade-offs that can be made based on control system size and desired performance. The H_∞ controller is combined in parallel with the integral controller for this thesis. The analysis shows that the parallel combined controller outperforms all other controllers; however, the cost analysis shows that a simpler Zernike reduced model can achieve slightly reduced performance at a much lower cost.

14. SUBJECT TERMS MIMO control, Robust control, adaptive optics, segmented mirrors, flexible structures, space telescopes, Shack-Hartmann sensors, hybrid controller			**15. NUMBER OF PAGES** 95
			16. PRICE CODE
17. SECURITY CLASSIFICATION OF REPORT Unclassified	**18. SECURITY CLASSIFICATION OF THIS PAGE** Unclassified	**19. SECURITY CLASSIFICATION OF ABSTRACT** Unclassified	**20. LIMITATION OF ABSTRACT** UU

NSN 7540-01-280-5500 Standard Form 298 (Rev. 8-98)
Prescribed by ANSI Std. Z39.18

THIS PAGE INTENTIONALLY LEFT BLANK

Approved for public release; distribution is unlimited

COMBINED INTEGRAL AND ROBUST CONTROL OF THE SEGMENTED MIRROR TELESCOPE

Michael W. Looysen
Lieutenant, United States Navy
B.S., United States Naval Academy, 2000

Submitted in partial fulfillment of the
requirements for the degree of

MASTER OF SCIENCE IN ASTRONAUTICAL ENGINEERING

from the

NAVAL POSTGRADUATE SCHOOL
December 2009

Author: Michael W. Looysen

Approved by: Dr. Brij Agrawal
Thesis Advisor

Dr. Jae Jun Kim
Co-Advisor

Dr. Knox T. Millsaps
Chairman, Department of Mechanical and Astronautical Engineering

THIS PAGE INTENTIONALLY LEFT BLANK

ABSTRACT

Future space telescopes must maintain lower mass of the mirrors to keep launch cost down while increasing the size and performance of the space telescope. Although much work has been done in both adaptive optics and robust control, this thesis explores the application of several Multi-Input, Multi-Output controller designs for wavefront control of a Segmented Mirror Telescope with 936 actuators and 732 sensors. This thesis builds on previous robust control design by combining classical control with an H_∞ robust controller on a Singular Value Decomposition reduced model. It also presents reduction using Zernike polynomials and applies it to the integral control model as an alternate to Singular Value Decomposition model reduction.

All methods were able to meet the 10 Hz bandwidth by design. Therefore, the analysis shows that there are several trade-offs that can be made based on control system size and desired performance. The H_∞ controller is combined in parallel with the integral controller for this thesis. The analysis shows that the parallel combined controller outperforms all other controllers; however, the cost analysis shows that a simpler Zernike reduced model can achieve slightly reduced performance at a much lower cost.

THIS PAGE INTENTIONALLY LEFT BLANK

TABLE OF CONTENTS

LIST OF FIGURES

LIST OF TABLES

THIS PAGE INTENTIONALLY LEFT BLANK

ACKNOWLEDGMENTS

I would like to express my appreciation to Distinguished Professor Brij Agrawal for the support and advisement while working on the research on this thesis. His assistance was invaluable to the completion of this research.

I would like to thank Dr. Jae Jun Kim for his time and assistance in the research of this thesis and through the thesis process. His guidance enabled me to successfully develop the complex models and research necessary to complete this thesis.

I would like to thank Dr. Hyungjoo Yoon for his expertise and assistance with the Robust Control concepts and instruction on this advanced control technique. His assistance was pivotal in achieving the foundations needed to move this research forward.

Finally, I would like to express my gratitude to my family and friends for the support and encouragement while working on this thesis.

THIS PAGE INTENTIONALLY LEFT BLANK

.

I. INTRODUCTION

A. MOTIVATION

Optics have been used in space since humans began building satellites in the 1960s. Optical systems in space eliminate the atmospheric distortions on the light wave while looking into distant galaxies, and provide the ability to image and map the earth's surface. The disadvantage of putting optics in space is the cost incurred by launching heavy optical payloads with large mirrors and lenses. A large static mirror will require a lot of support structure and extremely precise machining to maintain a perfectly shaped mirror within the tight tolerances required to get higher resolution desired from a system with a large mirror. The purpose of the segmented mirror system is to use a lighter and less rigid structure, combined with sensors, and computerized controllers to control the surface of the mirrors to remove the various sources of distortion on the light to get a better picture. By reducing the weight, the cost to launch a larger mirror is reduced, giving better performance at a lower launch cost.

The angular resolution for an optical system defines the greatest angular separation between two objects that an aperture can resolve. Angular resolution is calculated by the Rayleigh Criteria in Equation (1.1), where θ is the minimum theoretical angular separation between two objects:

$$\theta = 1.22 \frac{\lambda}{D_{aperture}} \tag{1.1}$$

As the diameter of the aperture increases, the angle between two objects can decrease and still be detectable. This means that far objects, such as stars, planets, and galaxies, can be closer together and still be distinguished. Using this equation and some geometry, the ground separation distance is also shown to be increased. In Figure 1, R is the distance to the ground from the aperture and D is the diameter of the aperture.

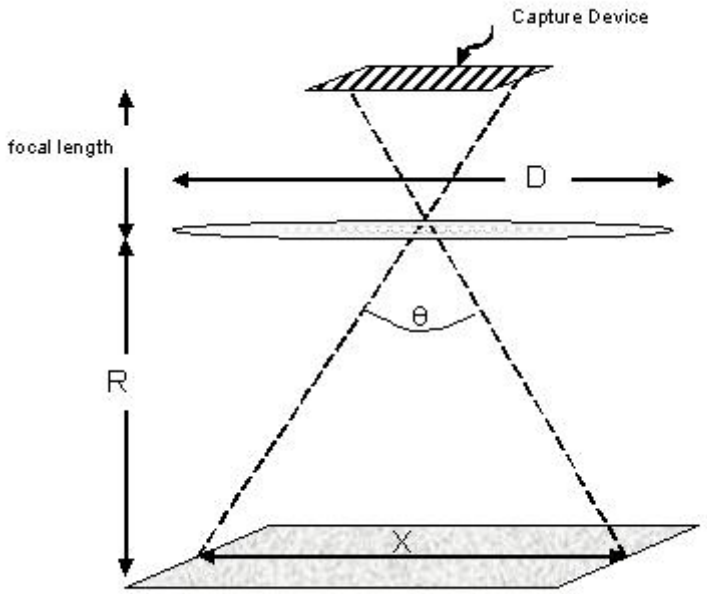

Figure 1. Ground separation distance

By using the calculations from reference [1], if the approximation of an angle:

$$\theta \approx X / R \tag{1.2}$$

is substituted in Equation (1.1), then Equation (1.3) holds as the distinguishable distance between two objects on the ground, also known as the ground separation distance.

$$X = 1.22 \frac{\lambda R}{D_{aperture}} \tag{1.3}$$

By increasing the diameter of the mirror, the ground separation distance can be decreased, which results in better theoretical maximum resolution of the system. In order to achieve a larger mirror in space, a segmented mirror is the most obvious choice since it can be folded up to fit within a launch fairing and deployed on orbit.

In addition to the increased resolution, segmented mirrors are also potentially more reliable and have a lower lifetime cost. For example, the Hubble

Space Telescope, launched in 1990, orbits the earth at 576 km and is capable of sensing from UV to near-Infrared frequencies of light. It has a 2.4-meter Ritchie-Chretien Cassegrain primary mirror. When it was launched in 1990, a spherical aberration was discovered in Hubble's primary mirror [2]. In 1993, the Corrective Optics Space Telescope Axial Replacement (COSTAR) was installed to correct the primary mirror aberration. The costs and time required to plan and conduct a servicing mission could have been reduced and the three years to correct the optical system could have been useable at the same or higher performance if the errors in the mirror could have been removed by having controllable segmented mirrors with adaptive optics.

The trade-off between a single, monolithic mirror and a series of smaller segmented mirrors is an increased complexity of the system. Although there are risks with a large continuous mirror having a defect or being out of tolerance, the complexity of controlling multiple mirrors is a large challenge to overcome. Several computer controllers are used in conjunction with multiple sensors and actuators. The James Webb Space Telescope (JWST) is NASA's next generation infrared-optimized telescope, scheduled to launch in 2014, shown in Figure 2.

Figure 2. James Webb Space Telescope (from [2])

The James Webb Space Telescope is a 6.5-meter diameter segmented mirror design, and will be launched to the L2 Lagrange Point on the opposite side of the earth from the sun. The primary optic is composed of 18 segmented hexagonal mirrors and a large sun shield, which will be folded and deployed after launch. Upon deployment, according to NASA's Jet Propulsion Laboratory, there are three major tasks that must be performed to ensure that the telescope works within the tight tolerances required to ensure good picture quality [3]. First, the satellite must be *Initialized* to conduct the initial alignment and figure correction control. This phase consists of coarse alignment of the segments, followed by fine phasing to correct the mirrors to a higher accuracy than can be achieved with coarse control. The next phase of *Calibration* must be done to establish influence functions and offsets needed for calculations for the last phase of *Maintenance*. During the maintenance phase, normal operations are conducted correcting for the wave-front error and "long-term monitoring and periodic correction of image quality" [3]. Much research has been done on the Alignment phase of control of the space segmented mirror as shown in reference [3] and [4], which discuss the coarse and fine control of the mirrors. The James Webb Space Telescope uses coarse and fine sensors for the alignment phase. It uses a science camera combined with other techniques for the "maintenance" phase. Other segmented telescope applications use a separate sensor, which will be discussed later, to detect the wave-front errors for correcting the optical picture in the maintenance phase.

An earth imaging segmented mirror has a different concept of operations than a deep space imaging system like the JWST. The JWST will be maneuvering less frequently than an earth imaging satellite. Since the earth imaging satellite will be moving more, it will have more sources of input noise to the optical system from sources such as attitude control system or the changing thermal gradients across the mirror surface. The JWST controls the thermal issue by using a large sunshade to block the sun from the mirrors and satellite structure, which is relatively easy since it will be in an orbit at a Lagrange point

and the sun will always be in the same position relative to the satellite. It would be much more difficult to have a continuously controlled or enormous sunshield to shade mirrors when looking at the earth, which is nullified by the fact that there is energy reflected off the earth's surface in the form of albedo. Also, the earth has an infrared signature that is absorbed by a satellite and cannot be shielded when looking at the earth. Therefore, it is necessary for an earth-viewing satellite to have more control over the wavefront when looking at the surface of the earth than a satellite looking at deep space or at galaxies far, far away.

B. Objectives

The objective of this thesis is to develop a control system to correct the wavefront error. It is assumed that the coarse and fine control of the system has been done and will continue to be done by a separate controller and only the wavefront error must be corrected to achieve surface figure control. This thesis will show that by using an integral controller combined with robust control techniques, better bandwidth and greater control of the system can be achieved than by either robust or classical control alone.

C. Overview

Chapter II presents a background in adaptive optics systems and control systems for adaptive optics. This chapter presents the principles of adaptive optics systems including the sensors and actuators used to control a wavefront for precise imaging.

Chapter III is a description of the Segmented Mirror Telescope, including system identification. This chapter describes the system on which the thesis research was based in order to gain an understanding of how the control systems were applied.

Chapter IV describes classical and robust controls as applied to the segmented mirror telescope. This chapter further explains how the control

systems can be combined to create a combined classical and robust control system for use in a multi-input multi-output (MIMO) system as applied to the segmented mirror telescope.

Chapter V presents the cost and performance measures used in evaluating the control systems and the results of the simulations. The results are analyzed and importance of the findings from the design and simulation are discussed.

Chapter VI discusses the summary, conclusion and future work to continue the work done on this thesis.

II. BACKGROUND

A. ADAPTIVE OPTICS SYSTEMS

Adaptive optics is based on using a light "wavefront" that has been distorted in some way and applying control to the optical path of the telescope to correct for the aberrations. Although it is not always a physical reality, it is assumed in adaptive optics that light emitted from a surface travels as a flat wave. Imagine light at a specific instance in time being reflected from a surface at exactly the same speed and time. If it is going through a vacuum without any interference, it will arrive at a flat sensor as a flat wave and precisely the same as it left the surface. Of course, this is not possible in reality because of multiple sources of distortion that the light will undergo as it travels from the source to the sensor. The spreading of the light from a spherical surface is also ignored, due to difficulties in reconstructing a wavefront as a curved surface and not a flat surface.

One of the sources of the distortion is the atmosphere. Light refracts when it transitions between mediums with different index of refractions, as defined in Snell's Law of Refraction in Equation (2.1), where θ_1 and θ_2 are the angle before and after transitioning through different "parts" of the atmosphere.

$$\frac{\sin\theta_2}{\sin\theta_1} = \frac{\eta_1}{\eta_2} \tag{2.1}$$

The indices of refraction, η_1 and η_2, are indirectly proportional to the speed of light through the specific medium based on the frequency of the light and the number of free electrons per unit volume, N.

$$\eta = \sqrt{1 - \frac{80.6 \bullet N}{f^2}} \tag{2.2}$$

Since the number of free electrons in the atmosphere is constantly changing and are asymmetrically distributed even within the same layers of the atmosphere, light will be constantly refracting throughout its path through the atmosphere.

Aside from the external distortions on light, there are often sources of aberration internal to the optical system, including physical defects or imperfections in the optical components, such as mirrors and lenses. Defects in the lenses such as uneven coatings and slight imperfections in the glass of the lenses can cause aberrations. Mirrored systems can have polished surfaces that are imperfect or out-gassing from components in space can collect on the mirror causing a difference in reflection on the surface of the mirror. Micrometeorites could cause the mirror to become slightly scratched or pitted. All of these sources of distortion cause a wavefront that would otherwise be flat to distort and change shape in some way. The nature of decreasing the mass of the mirror adds additional complexity to the control with the lower natural frequencies in the system than an extremely rigid structure. The problem with lower natural frequencies is that more active control will have to be done on the system to control the lower frequency to get them to damp out and reduce error in a reasonable time. Also, as discussed before, depending on the application, there can also be a thermal disturbance on the mirrors, which will cause a distortion if not corrected.

1. Wavefront Estimation

a. Zernike Polynomials

With the knowledge that the atmosphere and other factors distort the light coming into the lens, it was necessary to develop a way to mathematically describe the wavefront in order to control it. The Zernike polynomials accomplish this through a series of coefficients that describe the

phase of the light. The normalized Zernike polynomials are generally described by Equation (2.3), which is normalized over the unit circle by dividing the radius ρ by the maximum radius, R' [5].

$$R_n^m\left(\frac{\rho}{R'}\right)=\sum_{s=0}^{\frac{n-m}{2}}(-1)^s\frac{(n-s)!}{s!\left(\frac{n+m}{2}-s\right)!\left(\frac{n-m}{2}-s\right)!}\left(\frac{\rho}{R'}\right)^{n-2s} \tag{2.3}$$

And the phase of the wavefront is calculated as [5]:

$$\Phi(\rho,\theta)=A_{00}+\frac{1}{\sqrt{2}}\sum_{n=2}^{\infty}A_{no}R_n^0\left(\frac{\rho}{R'}\right)+\sum_{n=1}^{\infty}\sum_{m=1}^{n}\left[A_{nm}\cos m\theta+B_{nm}\sin m\theta\right]R_n^m\left(\frac{\rho}{R'}\right) \tag{2.4}$$

This phase describes the wave advance or retardation, which can be thought of as the height with respect to the planar wavefront.

Normally, the Zernike polynomials are derived in the polar form, but can be transformed into Cartesian coordinates using the relationships in Equations (2.5) and (2.6).

$$\rho=\sqrt{x^2+y^2} \tag{2.5}$$

$$\theta=\tan^{-1}\left(\frac{x}{y}\right) \tag{2.6}$$

The first 24 Zernike polynomial terms are shown in Table 1 in the Cartesian coordinate system.

Table 1 shows the increasing order of polynomial coefficients. There is an inverse relationship between the coefficients of the Zernike polynomials and the amount of influence that they have on the wavefront. The lower the order of polynomial coefficients, the more influence the particular coefficient has over the wavefront, similarly to eigenvalues or singular values. This will be important later when creating a modal control model.

Table 1. Zernike Polynomials (after [6])

#	n	m	Polynomial	Term
0	0	0	1	Piston
1	1	1	x	Tilt x
2	1	1	y	Tilt y
3	1	0	$-1 + 2 (x^2 + y^2)$	Power
4	2	2	$x^2 - y^2$	Astigmatism x
5	2	2	$2 x y$	Astigmatism y
6	2	1	$-2 x + 3 x (x^2 + y^2)$	Coma x
7	2	1	$-2 y + 3 y (x^2 + y^2)$	Coma y
8	2	0	$1 - 6 (x^2 + y^2) + 6 (x^2 + y^2)^2$	Primary Spherical
9	3	3	$x^3 - 3 x y^2$	Trefoil x
10	3	3	$3 x^2 y - y^3$	Trefoil y
11	3	2	$-3 x^2 + 3 y^2 + 4 x^2 (x^2 + y^2) - 4 y^2 (x^2 + y^2)$	Secondary Astig x
12	3	2	$-6 x y + 8 x y (x^2 + y^2)$	Secondary Astig y
13	3	1	$3 x - 12 x (x^2 + y^2) + 10 x (x^2 + y^2)^2$	Secondary Coma x
14	3	1	$3 y - 12 y (x^2 + y^2) + 10 y (x^2 + y^2)^2$	Secondary Coma y
15	3	0	$-1 + 12 (x^2 + y^2) - 30 (x^2 + y^2)^2 + 20 (x^2 + y^2)^3$	Secondary Spherical
16	4	4	$x^4 - 6 x^2 y^2 + y^4$	Tetrafoil x
17	4	4	$4 x^3 y - 4 x y^3$	Tetrafoil y
18	4	3	$-4 x^3 + 12 x y^2 + 5 x^3 (x^2 + y^2) - 15 x y^2 (x^2 + y^2)$	Secondary Trefoil x
19	4	3	$-12 x^2 y + 4 y^3 + 15 x^2 y (x^2 + y^2) - 5 y^3 (x^2 + y^2)$	Secondary Trefoil y
20	4	2	$6 x^2 - 6 y^2 - 20 x^2 (x^2 + y^2) + 20 y^2 (x^2 + y^2) + 15 x^2 (x^2 + y^2)^2 - 15 y^2 (x^2 + y^2)^2$	Tertiary Astig x
21	4	2	$12 x y - 40 x y (x^2 + y^2) + 30 x y (x^2 + y^2)^2$	Tertiary Astig y
22	4	1	$-4 x + 30 x (x^2 + y^2) - 60 x (x^2 + y^2)^2 + 35 x (x^2 + y^2)^3$	Tertiary Coma x
23	4	1	$-4 y + 30 y (x^2 + y^2) - 60 y (x^2 + y^2)^2 + 35 y (x^2 + y^2)^3$	Tertiary Coma y
24	4	0	$1 - 20 (x^2 + y^2) + 90 (x^2 + y^2)^2 - 140 (x^2 + y^2)^3 + 70 (x^2 + y^2)^4$	Tertiary Spherical

2. Optical Corrective Systems

To correct the aberration errors on the wavefront, yielding a better image, adaptive optics was developed. Although adaptive optics components vary from system to system, one of the most common adaptive optics systems is shown in Figure 3.

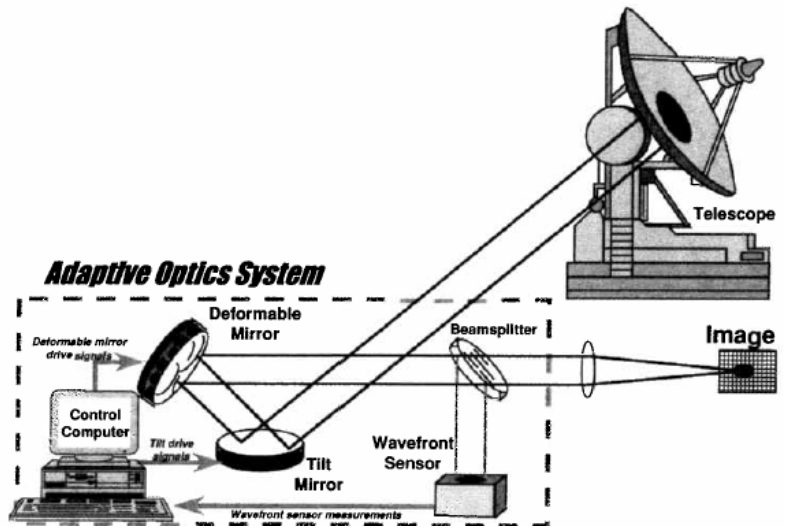

Figure 3. Common Adaptive Optics System (from [5])

Although adaptive optics has been historically used on terrestrial telescopes to correct for aberrations from the earth's atmosphere when looking at stars, it can also be applied to space telescopes to correct for the additional sources of error as discussed. A more detailed schematic of the adaptive optics system is shown in Figure 4. This figure shows the control computer in more detail and both the reference beam path and the object path.

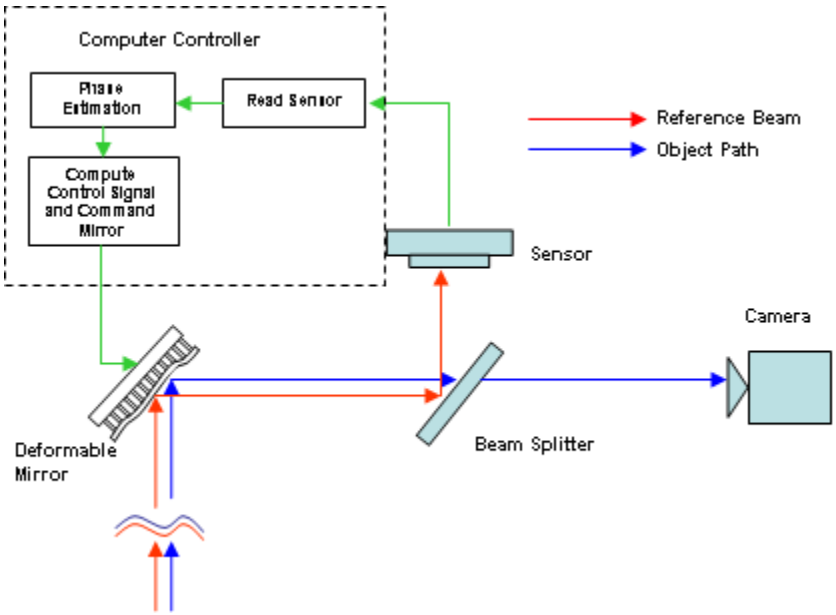

Figure 4. Adaptive Optics Schematic (from [7])

The basis for many adaptive optics systems lies on the principle of phase conjugation [5]. Electromagnetic waves are made up of both a phase and an amplitude and a wavefront can be described by Equation (2.7), where A is the amplitude of the wave and ϕ is the phase of the wave.

$$E = A \bullet e^{-i\omega t} = A \bullet e^{-i\phi} \tag{2.7}$$

To counter the effects of distortion of the wavefront, adaptive optics reverses the phase of the wave. This is called phase conjugation because in effect, the complex conjugate of the electromagnetic wave is achieved by reversing the sign before the imaginary component of the exponent [5].

3. Wavefront Sensors

In order to be able to remove these phase distortions, the system must be able to measure the phase of the wavefront. This is done in the "sensor" block of Figure 4 and is called the "wavefront" sensor. There are several types of wavefront sensors currently used, including shearing interferometers and Shack-Hartmann sensors. The Shack-Hartmann sensor will be the focus in this thesis

because of the specifics of the system analyzed, which will be discussed in Chapter III. A schematic of the Shack-Hartmann sensor is shown in Figure 5.

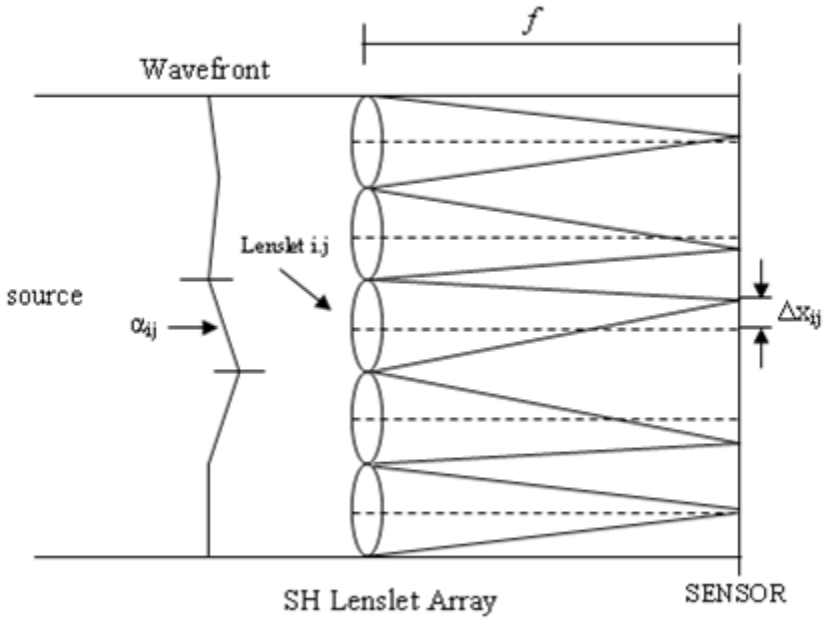

Figure 5. Shack-Hartman Lenslet Array (after [7])

The Shack-Hartmann sensor is composed of a series of lenslets in a flat array. When light passes through a lens it is focused on the CMOS sensor behind the lenslet array. The measurement of the displacement, Δx, is used to calculate the angle that the light hits the lens, known as the slope of the wavefront, which is used to calculate the phase of the light. These lenslets are arranged in an array to give a two-dimensional picture of the planar wave as it hits the array of lenslets and projects onto the CMOS sensor behind the lenslet grid. This array of phases is used to correct the wavefront using the different options available for wavefront correction, which is most often the deformable mirror in adaptive optics.

4. Controllable Mirrors

a. Tip/Tilt Mirror

The purpose of the tip/tilt mirror is to remove the wavefront tilt. The tilt is the average slope of the wave, and the tip/tilt mirrors serve as pointing for the main “beam” of light. The tip/tilt mirror is for coarse control of the light onto the wavefront sensor, e.g., the Shack-Hartmann sensor. The finely controlled, localized slopes are removed using a deformable mirror.

b. Deformable Mirrors

The deformable mirrors act as a finely controlled sheet of actuators and a mirrored surface or surfaces. They come in several different types, such as multiple segmented mirrors that have individual up/down or tip/tilt actuators or a continuous facesheet that have multiple actuators warping and bending the mirror surface to remove the wavefront errors as shown in Figure 6.

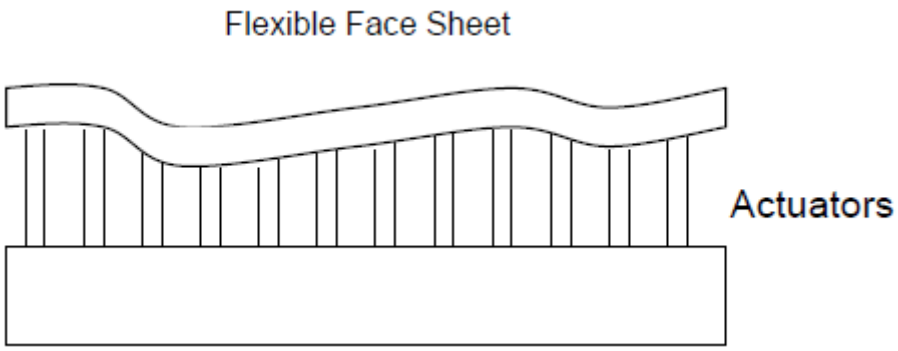

Figure 6. Deformable Mirror (from [8])

The advantage of the deformable mirror is that they have a 100% fill factor to remove the aberrations in the wavefront. A disadvantage of these mirrors is the coupling of the modes. When one of the actuators bends the facesheet, it influences the nearby surface of the mirror to move. This can be a problem if the corrected value of the nearby surface should be different than the influenced value and another actuator must be induced to counter the effect, which causes influences to the area surrounding the second actuator. This effect

ripples throughout the mirror, and eventually can cause problems with control of the mirror caused by induced modes. This coupling will also reduce the bandwidth of the controller.

B. ADAPTIVE OPTICS CONTROLS

As previously stated, an adaptive optics system relies on three primary things: wavefront sensors, controllable mirrors, and a computer controller. The computer controller will utilize the readings from the wavefront sensors to apply a control law and create command signals to the actuators. These command signals are most often voltages to drive the actuators to a specific position.

There are typically multiple loops in the control law for the adaptive optics system: coarse control, fine control, and facesheet control, as shown in Figure 7, where the actuators, sensors and physical components of the adaptive optics system are part of the Plant, G(s).

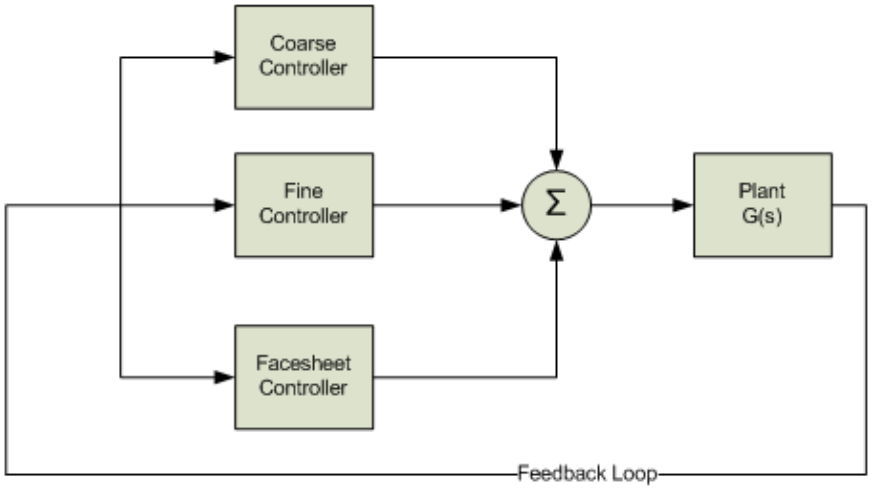

Figure 7. General Segmented Space Telescope Control

Each of these control loops uses one or a combination of all of the sensors to control the different actuators. Coarse control uses gap sensors to conduct the initial alignment of the mirrors. This is the first step in calibrating an electro-optical system. Fine control primarily uses the tip/tilt sensors and controls

tip/tilt mirrors to reduce the first order aberrations. Facesheet control primarily uses the Shack-Hartmann sensors and controls the facesheet actuators shown in Figure 6. Facesheet control removes the higher order wavefront aberrations. These three control types are not always distinct in each system, depending on the application of adaptive optics. For example, the James Webb Space Telescope conducts a calibration phase and operates in fine control mode, but does not use a deformable mirror for wavefront correction; it uses a tip/tilt control mirror.

The first step to generating a control law is to use a method for recreating the phase of the wavefront. This is done using either a modal or zonal method, as described in [9]. The modal method uses a modal representation, most often Zernike Polynomials, for wavefront reconstruction. The zonal method uses the physical coordinates for the estimation. Once the phase of the wavefront is calculated, it can be removed by phase conjugation or other methods. Phase conjugation is the process by which the phase from Equation (2.7) is reversed, or negated. Practically, the phase can be thought of as the distance from the axis average of the wavefront. The first-order aberration, removed by the tip/tilt mirror in the fine control phase, is the average slope of the wavefront. The higher order aberrations are the “local” slopes of the wavefront, as measured by the Shack-Hartmann sensor at each geographic lens position. The phases at these local positions are the distances from the average position of the entire wavefront. The phases are “conjugated” by adjusting the deformable mirror to exactly negative of the measured phase, allowing for a phase shift, in effect “flattening” the wave. The process is shown in Figure 8.

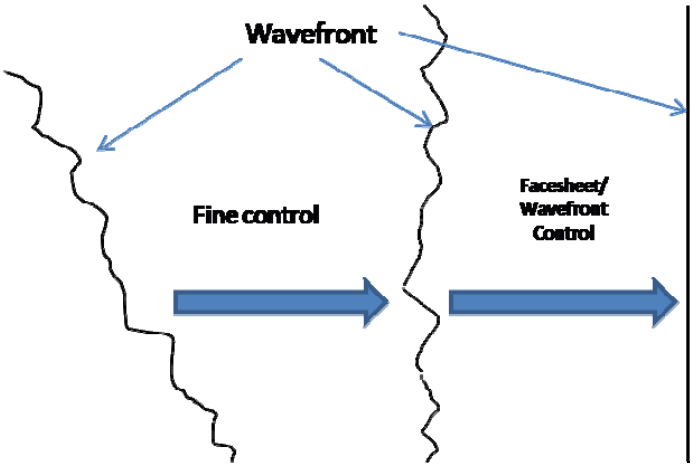

Figure 8. Wavefront Control

THIS PAGE INTENTIONALLY LEFT BLANK

III. SEGMENTED MIRROR TELESCOPE

A. SYSTEM DESCRIPTION

The analytical model used in this thesis is a segmented mirror telescope consisting of six hexagonal segments arranged in the configuration shown in Figure 9. This system was developed and built for testing purposes, but never intended for flight. No work for this thesis was done on the actual hardware, only the state-space representation of the mathematical model was provided in the Matlab format.

The center hexagon is left open for light to reflect off a secondary mirror to be collected by an optical receiver in the center in the same way that the JWST operates.

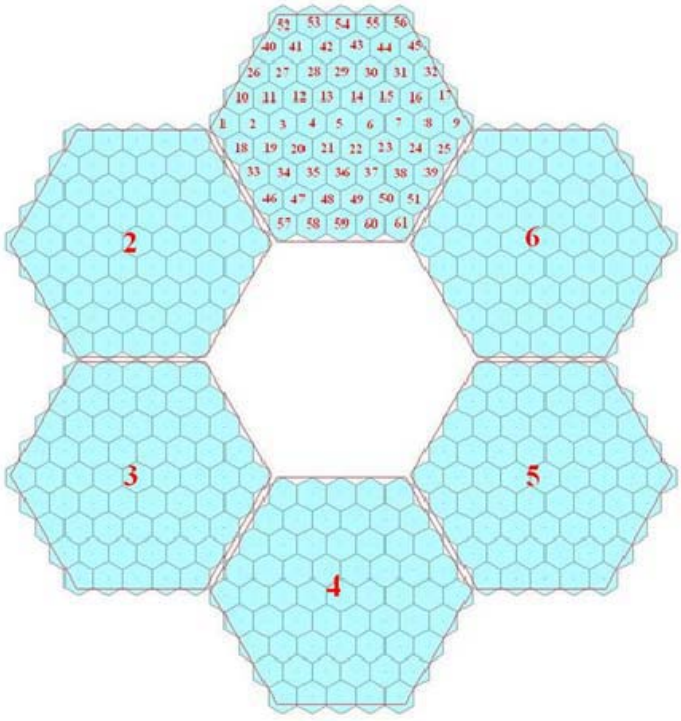

Figure 9. Segmented Mirror Lenslet Orientation (from [7])

The lenslets shown are the corresponding lenslets from the Shack-Hartmann Sensor. As shown in Figure 9, there are 61 lenslets in each of the six

Shack-Hartmann sensors, for a total of 366 lenslets. Each hexagonal mirror has 156 facesheet actuators, giving a total of 936 actuators. The primary mirrors are deformable by use of these actuators, and there is not another deformable mirror in the optical path. In addition to the Shack-Hartmann sensor, there are phase diversity, gap, and jitter sensors. These sensors are used in the fine control phase of the segmented mirror, but are not used for facesheet control. The fine control, bipod, and Fast Steering Mirror (FSM) actuators are used for fine control.

B. SYSTEM IDENTIFICATION

The plant model used for this thesis is a state-space model, which characterizes the system dynamics and physical relationships mathematically. The state space is in the form in Equation (3.1).

$$\begin{aligned} \dot{x} &= Ax + Bu \\ y &= Cx + Du \end{aligned} \tag{3.1}$$

The $\vec{x}$ term is a vector of the states and $\vec{u}$ is a vector of the control inputs to the system. The *A* matrix represents the linear combination of states physically present in the entire Segmented Space Telescope system. There are 332 states in this system, therefore the size of the *A* matrix is [332 x 332] elements. The *B* matrix represents the actuator inputs to the system. Since the Segmented Space Telescope has a total of 997 actuator inputs, and the inputs are coupled, the size *B* matrix is [332 x 997] elements. The output of the system is dictated by the bottom term of Equation (3.1). The *C* matrix represents the sensor outputs of the system. There are 936 outputs of the system, therefore this is a [936 x 332] matrix. In addition to the sensor outputs, this state-space model also outputs the position states of the model. These states are not physically measured in the real system, so it is not reasonable to use them for control of the system. The *D* matrix relates the inputs from the $\vec{u}$ vector to the outputs, similar to a feed-forward system, and is a [936 x 997] matrix.

Table 2 shows each input and output of the Matlab state-space model used for this thesis.

Table 2. Segmented Mirror Telescope Model Inputs and Outputs

INPUTS				
		Channels		
Name	**Total**	**From**	**To**	**Per Segment**
Face Sheet Actuators	936	1	936	156
Fine Control Actuators	18	937	954	3
Bipod Actuators	36	955	990	6
FSM Torque Actuators	2	991	992	
Base Shake Actuators	3	993	995	
FSM Angle Actuators	2	996	997	
OUTPUTS				
		Channels		
Name	**Total**	**From**	**To**	**Per Segment**
Shack-Hartmann Sensor	732	1	732	122
Gap Sensors	18	733	750	3
Jitter Sensor	2	751	752	
Phase Diversity	18	753	770	3
Position States Output	166	771	936	

The Shack-Hartmann sensor outputs were given as groups of x-slopes and y-slopes for each segment. The first 61 channels x 6 segments are x-slopes and the next 61 channels x 6 segments are y-slopes of the Shack-Hartmann Sensor. These slopes could be used to reconstruct the phases for purposes of wavefront visualization.

1. System Characteristics

The most important system characteristic that is necessary to be known is the natural frequency. The natural frequency of this system was obtained by finding the eigenvalues of the *A* matrix of the state-space model. The imaginary terms of the eigenvalues are the natural frequencies in radians per second. The lowest natural frequency for the Segmented Mirror Telescope system is at 29 Hz,

but the frequencies ranged up to 767 Hz. These frequencies include all supporting structural frequencies, as well as the frequencies in the flexible mirrors.

C. STATE-SPACE MODEL FOR WAVEFRONT CONTROL REDUCTION

For purposes of this thesis, it is assumed that the coarse and fine controllers are operating to remove the pointing and first-order aberrations to the wavefront. Therefore, the only sensors that will be used are the Shack-Hartmann sensors and the only actuators that will be used are the facesheet actuators.

State-space models are dependent on the relative sizes of the matrices. The basic pictorial view of the matrices are formatted in a block; the full model of the space segmented telescope is shown in Equation (3.2).

$$G_{full} = \left[\begin{array}{c|c} \underset{332x332}{A} & \underset{332x997}{B} \\ \hline \underset{936x332}{C} & \underset{936x997}{D} \end{array}\right] \tag{3.2}$$

To use the facesheet actuators for modeling and to build the control law, the *B* matrix was reduced to [332 x 936] and to use only the Shack-Hartmann sensors, the *C* matrix was reduced to [732 x 332]. In order to maintain the necessary size of the state space, the *D* matrix was reduced to [732 x 936]. Although only the facesheet actuators and the Shack-Hartmann sensors were used, it is important to note that the system dynamics as modeled in the *A* matrix remained unchanged.

IV. SEGMENTED MIRROR TELESCOPE CONTROL METHODS

A. CLASSICAL CONTROL

1. Introduction

The purpose of a control system is to remove error from a system and achieve specific performance objectives of a system. The control system, or compensator, is created in software to use the sensors readings to create a control signal and create stability and improve the transient response of the system or steady state response of the system. To design the control system, the plant first must be mathematically modeled in a computer program, such as Matlab and Simulink. The general form of a unity feedback system including the plant and controller are shown in Figure 10.

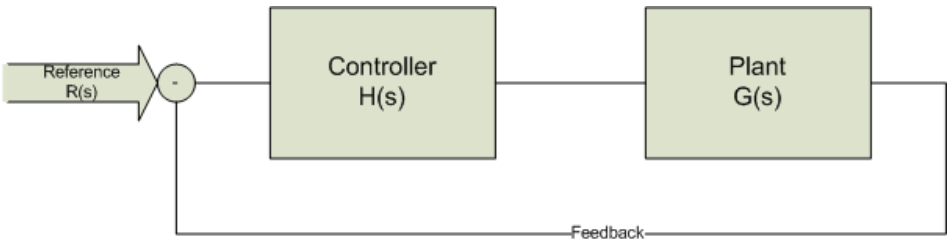

Figure 10. Control System Model

In a simple spring-mass-damper system, from Newton's second law, Equation (4.1) is the standard equation of motion, where U is the external force on the system.

$$m\ddot{x} + c\dot{x} + kx = U \tag{4.1}$$

In this case, the k/m term represents the square of natural frequency, and c/m represents the damping. Using this formula and Laplace transforms, the *proportional-plus-integral-plus-derivative (PID)* controller in Equation (4.2) can be created. Practically, K_i eliminates steady state error, K_d adjusts system damping, and K_p adjusts the system stiffness.

$$H(s) = \frac{K_i}{s} + K_p + K_d s \tag{4.2}$$

The PID controller for the Single-Input, Single-Output (SISO) case is modeled according to Figure 11.

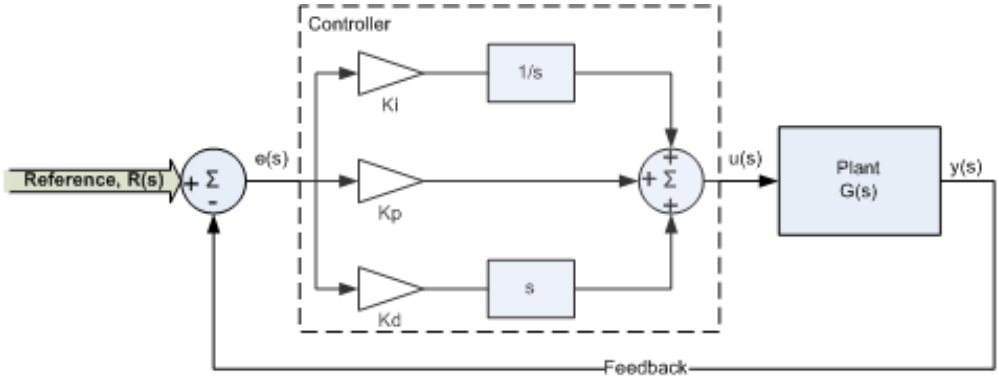

Figure 11. PID Controller

By using methods of classical control, such as root locus and bode plots to tune the gains, K_i, K_p, and K_d, the desired output of the plant, y(s), can be controlled to meet desired performance conditions. The typical performance conditions are desired settling time, steady state error, and control bandwidth. Control bandwidth is the frequency range at which the system output reasonably follows its desired reference. Bandwidth is calculated as the frequency at which the magnitude response curve, or Bode plot, of the closed loop system crosses -3 dB in magnitude.

The compensator used in this thesis is a purely integral control, meaning that only K_i and the integrator are used for control and the other loops are not used.

a. Frequency Response

Frequency response tools are very useful when characterizing system dynamics and designing a control system. Among the most useful frequency response techniques are bode plots and root locus plots for SISO systems.

The root locus is used to determine stability of the system. It is a plot of the poles of the system on vertical imaginary axis and horizontal real axis.

In order for the system to be stable, the closed loop system must not have any poles in the Right-Half Plane (RHP) on the root locus plot.

The plot of the magnitude and phase versus frequency is called the Bode plot. This plot is useful for determining where the instability in the system identified by the root locus exists. If the magnitude of the bode plot is greater than 0 dB at frequencies where the phase plot passes below -180 deg, the system is instable. This information is useful when determining what frequencies to design the filters to remove.

2. Multi-Input, Multi-Output (MIMO)

The Segmented Mirror Telescope model used in this thesis is a multi-input, multi-output (MIMO) system. At the most basic level, a MIMO system can be thought of as a series of mass-spring-damper systems. However, a MIMO system behaves differently than a SISO system due to coupling of the inputs. Each of the segmented mirrors has 156 facesheet actuators and 61 Shack-Hartmann lenslets, so each of the actuators has an effect on the wavefront sensed by more than one lenslet. The system is modeled as a state-space representation and, although the general theory of integral control can be used for control of the mirrors, the implementation of the control system is slightly different.

As discussed in Chapter II, in order to control the wavefront error, the traditional way of controlling the wavefront error included recreating the wavefront, then applying the conjugate phase to remove the errors. In this thesis the wavefront is not recreated for conjugate phase control. Instead, the controller seeks to create a flat wavefront by controlling the slopes of the wave to zero. The slopes of the wave are immediately known by the output of the Shack-Hartmann sensor, so the use of Zernike polynomials or other methods to recreate the wavefront are unnecessary for control of the mirrors. The Zernike coefficients themselves can be used for control, which will be discussed later.

Although the slopes of the wavefront are known, the error is not directly related to the inputs, meaning that since the inputs and outputs are coupled, it becomes necessary for integral control to have a relationship of inputs to outputs as part of the control path. This can be done with a steady-state gain (or DC gain) matrix in the control path that relates the inputs of the system to the outputs of the system. The Segmented Mirror Telescope model is represented in state-space format, G(s), as discussed. The minimal state-space realization of the plant can be represented using Equation (4.3).

$$G(s) = C(sI - A)^{-1}B + D \tag{4.3}$$

If a system has a fast response, the dynamics of the minimum realization can be ignored, represented by the sI term. The resulting G matrix is referred to as the *poke* matrix and is shown in Equation (4.4).

$$G_{poke} = C(-A)^{-1}B + D \tag{4.4}$$

Practically, the transfer matrix shown above relates the inputs of the system to the outputs of the system (ignoring dynamics). Therefore, in order to relate the output sensors to the actuator inputs for control, the inverse of G_{poke} is created as a matrix gain. In the case of the Segmented Mirror Telescope there are 936 inputs and 720 outputs; since this is not a square matrix, the pseudoinverse of G must be taken rather than the inverse.

Since the sensors have been translated to associated actuator inputs using the inverse of the poke matrix, the control on the actuators can be treated as a linear system. Using the same principles as the SISO integral control system, the gain, integrator, and a filter were added for control. The model for classical control used in this thesis is shown in Figure 12.

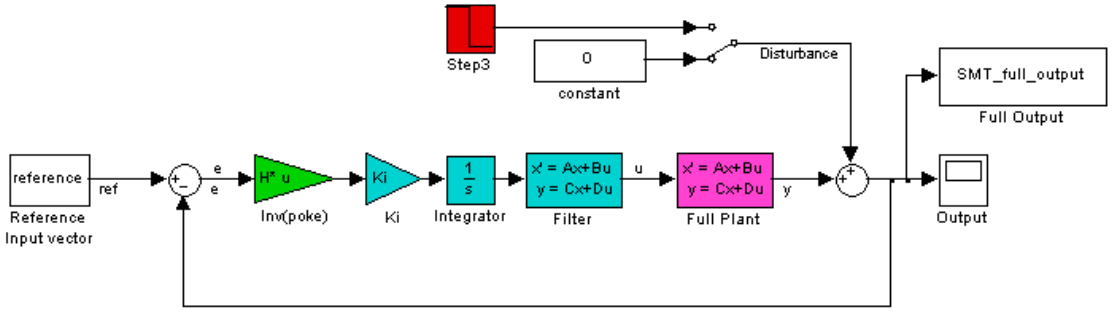

Figure 12. Simulink Classical Control Model

a. Model Reduction

The size of the plant and the associated control system presented problems with computer memory when designing and analyzing the control system for classical control. To create a plant that reasonably mimics the full sized plant for purposes of control system design, first it is necessary to use proven reduction techniques.

(1) Input/Output Reduction. Input/Output Reduction reduces the number of inputs and outputs to the system, but does not change the internal dynamics of the full system. There are two different bases for model reduction used in this thesis: Singular Value Decomposition and Zernike Polynomial Coefficient. Singular value decomposition is built on the premise that a matrix can be "decomposed" into three separate weighted matrices, as shown in Equation (4.5).

$$SVD(G) = U\Sigma V^T \tag{4.5}$$

The Σ matrix contains the most significant singular values, and the U and V matrices give the linear combination to transform the singular values back into the full G matrix. A plot of the singular values of the Poke matrix in Figure 13 shows that the first 100 singular values in this system are the most significant, therefore the system can be reduced to 100 inputs and outputs.

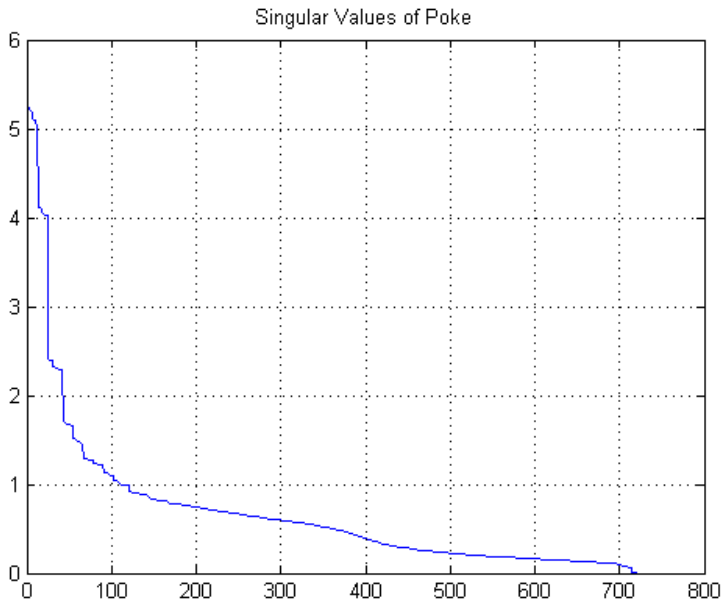

Figure 13. Singular Values of Poke Matrix

The reduction is accomplished by truncating the U and V matrices to the first 100 columns of the U matrix and first 100 rows of the V^T matrix. The reduced input/output state-space model is created using Equation (4.6).

$$G(s)_{new} = U^T{}_{reduced} G(s)_{full} V_{reduced} \tag{4.6}$$

An examination of the reduced G(s) reveals that it has 100 inputs, 100 outputs, and 332 states.

(2) System State Reduction. The system's states can be reduced in a similar way to the Input/Output reduction by using Hankel Singular Values. Hankel Singular Values are similar to the SVD-based input/output reduction, but are based on the observability and controllability grammians of the plant model. Using the methods outlined in [7], the Hankel Singular values of the Segmented Mirror Telescope are plotted in Figure 14.

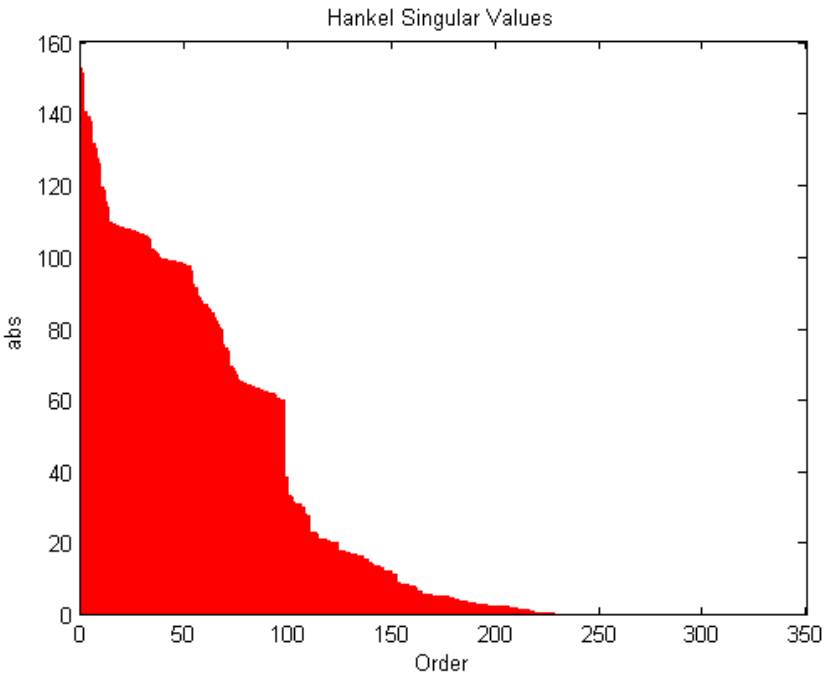

Figure 14. SMT Hankel Singular Values

This figure shows that although there are 332 states present in the system, it can be reduced to about 240 without losing any dynamics in the system since the Hankel Singular Values have zero influence on the system above 240. The reduction was done in Matlab using reduction algorithms and specifying to use Hankel Singlular Values. These reduced models are used to calculate the controller for H_∞ control synthesis.

b. Gain and Filter Tuning Using SVD Reduction

As described above, all tuning and testing was done on a plant reduced by the SVD method. To simplify this model, the K_i gain across all of the channels was assumed the same. The goal while tuning the gain was to create a stable system that meets the required bandwidth of 10 Hz. Using Matlab's robust control toolbox, a gain of less than 11 was required to produce a stable system, which is confirmed with the plot of the closed loop poles in Figure 15.

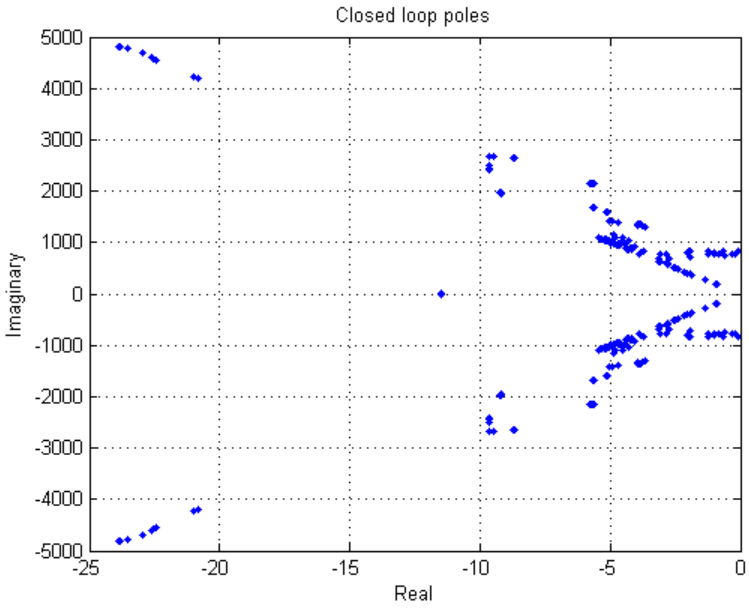

Figure 15. Closed Loop Poles of Integral Control System

Plotting the root locus for a MIMO system to check for stability is impractical, so a plot of the closed loop poles for the system is used instead. The existence of poles in the Right-Half Plane (RHP) of the closed loop pole plot would indicate that the system is unstable. Since all of the poles were in the Left-Half Plane (LHP), this system is stable.

Although the system is stable, the bandwidth at the max gain condition was only 1.8 Hz, therefore this does not meet the bandwidth requirements. To determine the frequencies that make the system unstable at higher bandwidths, the gain was increased to 64 to meet the 10 Hz bandwidth requirement. Although bandwidth is meaningless for an unstable system, by looking at the open loop bode plot in Figure 16, the regions of instability can be determined for this theoretical bandwidth. The bode plot of the unstable open loop system in Figure 16 confirm that there are several higher natural frequencies that are excited by the controller, yielding an unstable system with peaks above 0 dB where the phase crosses ± 180 degrees, which is an indicator of the region of instability frequencies.

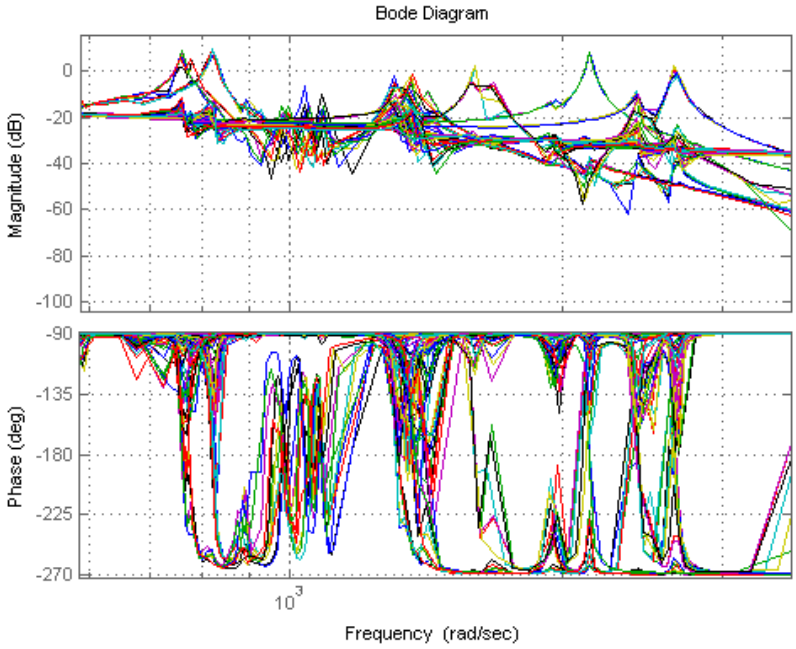

Figure 16. Open Loop Bode Plot of Unstable System

To control these natural frequencies, a filter must added to the control path to reduce the gain at higher frequencies, but allow the lower frequencies to have a higher gain for more control. Typically, the higher frequencies will naturally dampen out without control, as long as the lower frequencies are controlled adequately. All of the gains were adjusted for stable systems at nominal conditions only. No uncertainty or noise was added to the original model; therefore, the following adjustments were at the best case for the system.

(1) Notch filters. In order to bring the frequencies of concern below the 0 dB level and to improve performance, a notch filter is added at 239 Hz (1500 rad/sec) and a second notch filter is added at 29 Hz (183 rad/sec). These filters are second order transfer functions shown in Equations (4.7).

$$F(s) = \frac{s^2/\omega_z^2 + 2\zeta_z\, s/\omega_z + 1}{s^2/\omega_p^2 + 2\zeta_p\, s/\omega_p + 1} \tag{4.7}$$

For a notch filter, $\omega_z = \omega_p$ and the damping terms are chosen to determine the width and max gain of the notch according to Equation (4.8).

$$K_{\max} = 20\log_{10}(\zeta_z/\zeta_p) \tag{4.8}$$

The bode plot of the full fourth order, two-notch filter used is shown in Figure 17.

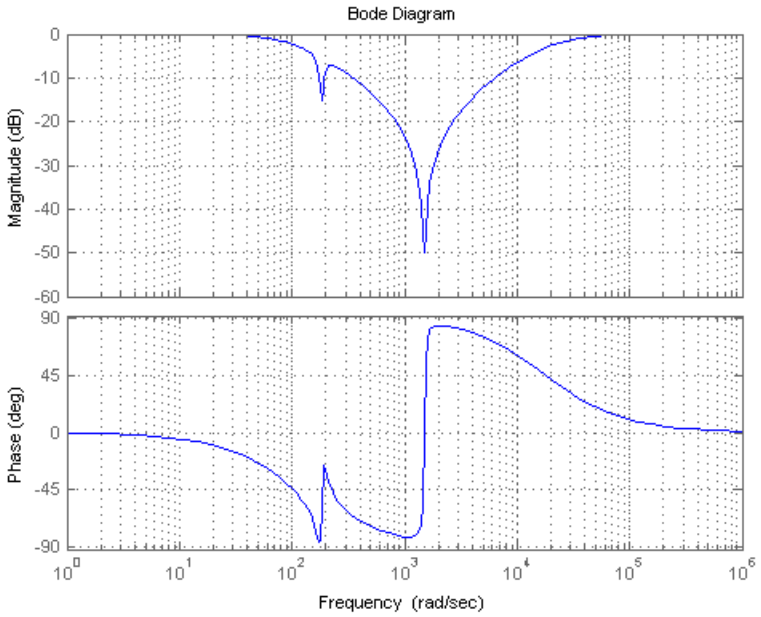

Figure 17. Notch Filters at 239 Hz and 29 Hz

This filter removed the higher frequencies, making the system stable, allowing the gain to be increased to 438 and the bandwidth to increase to 53 Hz, well within the requirement of 10 Hz. The plot of the closed loop poles in Figure 18 validates the system stability; there are no poles in the RHP of the closed loop pole plot in Figure 18, therefore this system is stable. The poles near the axis are stable, but proximity to the axis results in poor system performance.

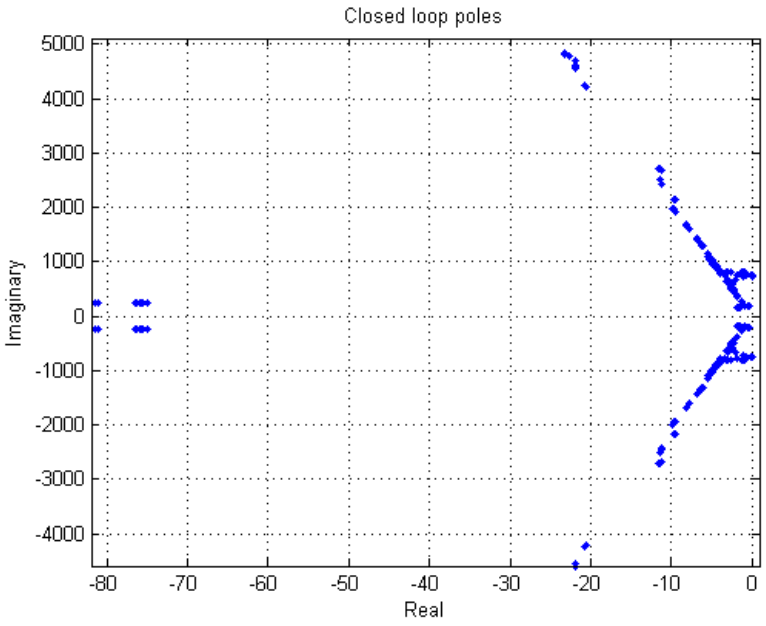

Figure 18. Closed Loop Poles, System with Notch Filter

To compare all of the classical control systems using the same metrics, each system was built in Matlab using the Control System Toolbox, then a step input was applied and the result read at the output. Although the system is stable and the bandwidth is within the requirements, this system step response to a unity reference input shown in Figure 19 has a long settling time.

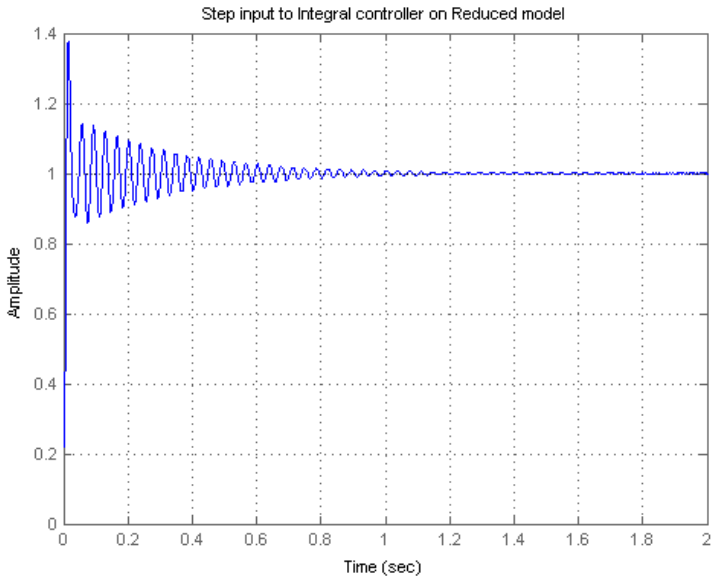

Figure 19. Notch Step Response at Maximum Stable Gain, Notch Filter

For a fast system, such as the Segmented Mirror Telescope, it is desired to have a fast settling time. By tuning the gain to get the best step response, better performance can be achieved and still meet the bandwidth requirement. The best gain to achieve the minimum bandwidth and best step response is 45. The step response is shown in Figure 20.

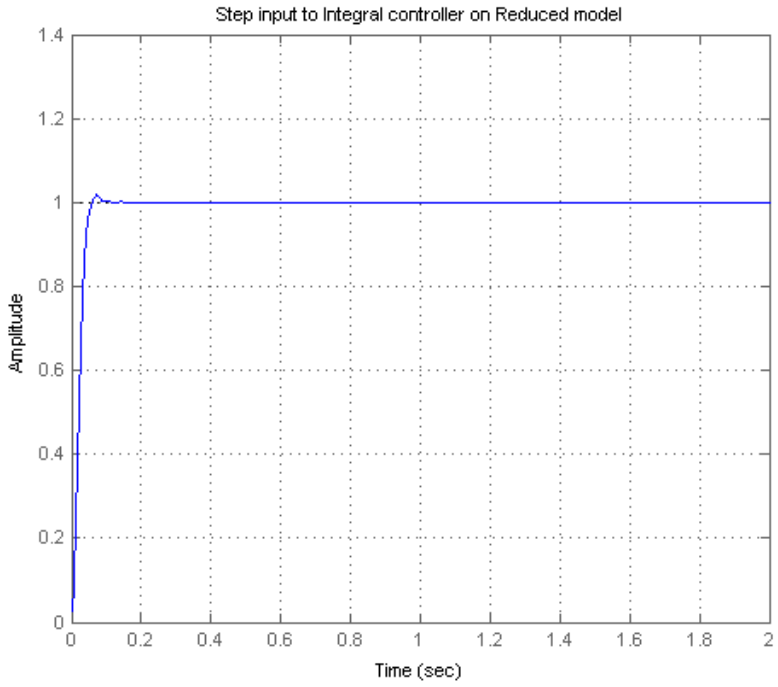

Figure 20. Step Response at Minimum Gain, Notch Filter

The two cases presented show the bounding cases for the gain on the system, which define the upper and lower limits of performance. The trade-off for better bandwidth is decreased performance in the step response.

(2) Elliptic Filter. The elliptic filter is another type of filter that can be used to decrease the frequencies in the area of interest. This filter has 0 dB gain at lower frequencies, then drops off at a cutoff frequency. It is typically a fourth or sixth order filter. This thesis explored the performance of two different sixth-order elliptic filters, one with a cutoff frequency at 29 Hz, and one with a cutoff frequency at 60 Hz. The 29 Hz cut-off frequency was chosen to try to get better performance by cutting off the frequency as close to the 29 Hz lower natural frequency as possible while allowing the lower frequencies to pass.

The bode diagram of the 29 Hz elliptic filter is shown in Figure 21.

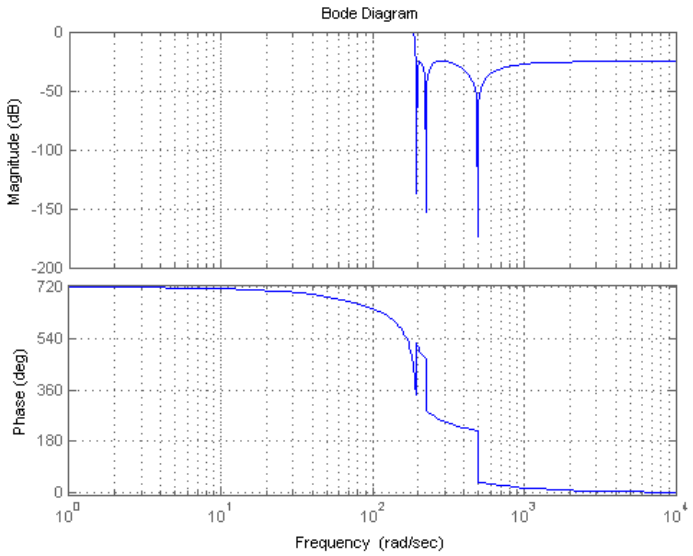

Figure 21. Elliptic Filter Bode Diagram, 29 Hz cut-off

The gains were tuned the same as with the notch filter, but the bottom of the curve was shown to be best to get a maximum bandwidth of 25.5 Hz using a gain of 113. This gain produces a very poor step response, as shown in Figure 22.

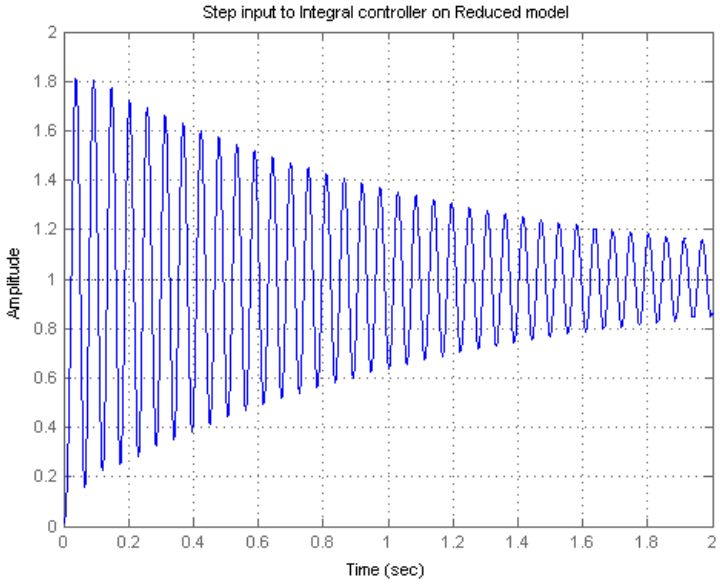

Figure 22. Step Response at Max Gain with Elliptic Filter, 29 Hz

The gain was again reduced to 33 to achieve the best performance at the required bandwidth of 10 Hz using the same elliptic filter. The step response is shown in Figure 23.

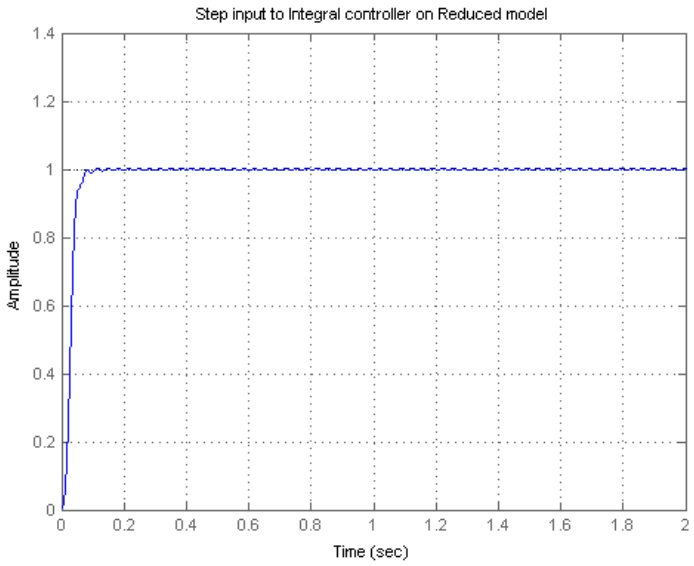

Figure 23. Step Response, Elliptic Filter, 29 Hz, Best Performance

This step response has a very fast settling time, but there is still a small initial sinusoidal resonance after it has reached steady state, which will eventually dampen out over time.

The bode plot of the elliptic filter with a 60 Hz cut-off frequency is shown in Figure 24. This frequency was chosen to achieve a higher bandwidth while still maintaining performance.

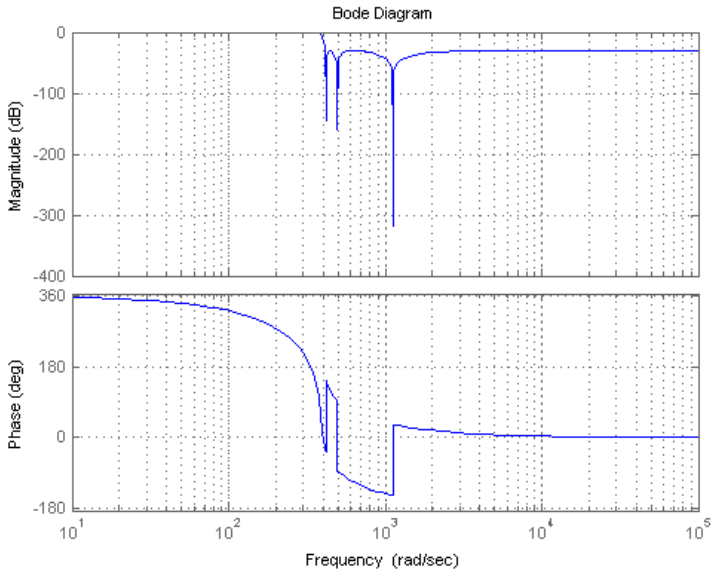

Figure 24. Elliptic Filter Bode Diagram, 60 Hz cut-off frequency

This system has a fast step response, but has a large overshoot and still has resonance, due to the 30 Hz natural frequency that is now in the pass band for the filter. This filter produces a significant increase in bandwidth to 44 Hz by using a gain of 133. The step response in Figure 25 shows the overshoot and a closer look in Figure 26 reveals the steady state resonance.

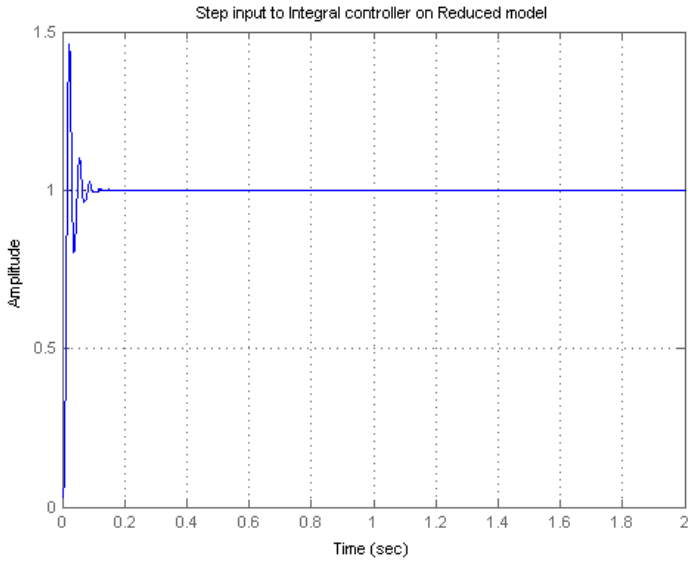

Figure 25. Step Response, Elliptic Filter, 60 Hz, Max Bandwidth

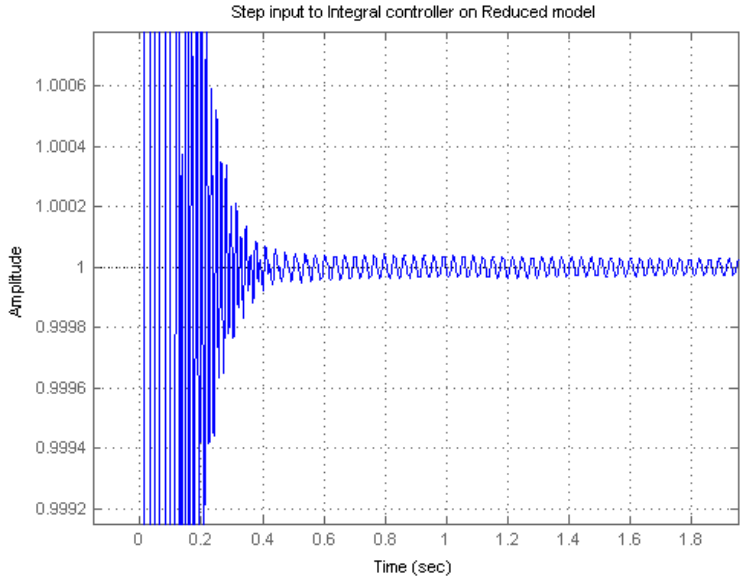

Figure 26. Step Response Magnification, Elliptic Filter, 60 Hz

The gain was reduced again in the same way it was done for the previous cases with the 30 Hz elliptic filter and the notch filter, and a gain of 45 produces a 10 Hz bandwidth. The performance was better than the max gain case, as shown in Figure 27.

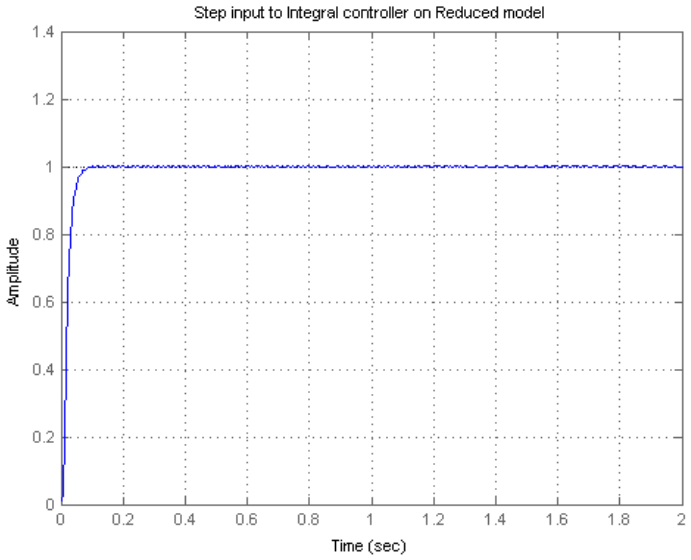

Figure 27. Step Response, Elliptic Filter, 60 Hz, Best Performance

Magnification to the same scale as Figure 26 shows that the steady state resonance is nearly gone, shown in Figure 28.

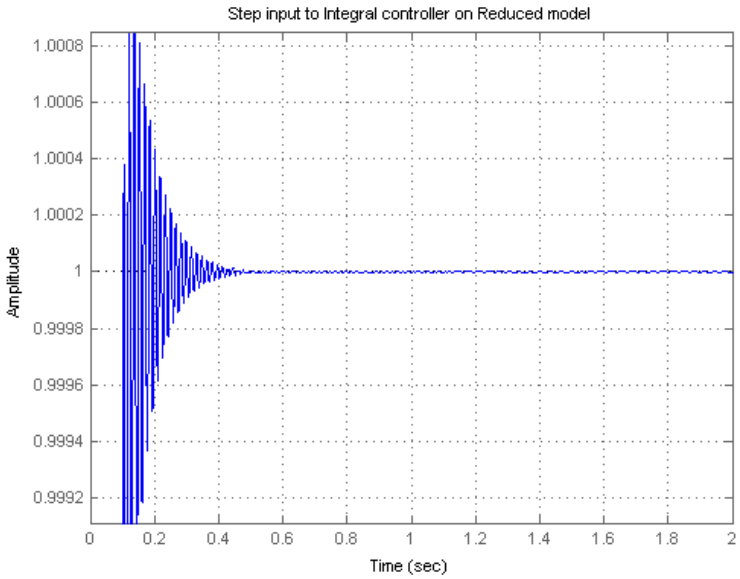

Figure 28. Step Response Magnification, Elliptic Filter, 60 Hz, Best Perf.

The classical control system for the Segmented Mirror Telescope requires a filter to meet the performance and bandwidth requirements. Three different filters were used in this thesis, a double-notch filter, an elliptic filter with 30 Hz cut-off and an elliptic filter with a 60 Hz cut-off frequency. Each of these filters produces adequate control and by adjusting the gain, the trade-off between performance and bandwidth can be made: better performance can be achieved at lower bandwidth or lower performance at higher bandwidth.

c. Zernike Polynomial Integral Control

Using the principles of Zernike Polynomials as discussed in Chapter II, the wavefront is related to the Shack-Hartmann wavefronts by Equation (4.9), where $\vec{y}$ is the vector of Shack-Hartmann sensor outputs, $\vec{a}$ is a vector of the Zernike polynomial coefficients, and [dZ] is a transfer matrix that maps the physical location of the Shack-Hartmann sensors to the Zernike polynomial coefficients.

$$\vec{y} = [dZ] \bullet \vec{a} \tag{4.9}$$

Since the use of Zernike coefficients is a set of weighted functions relating the Shack-Hartmann outputs to the most influential sensor combinations, this can be used for control of the modes of the system instead of directly controlling the desired Shack-Hartman outputs. This thesis used 21 Zernike coefficients for control. This system is shown in Figure 29.

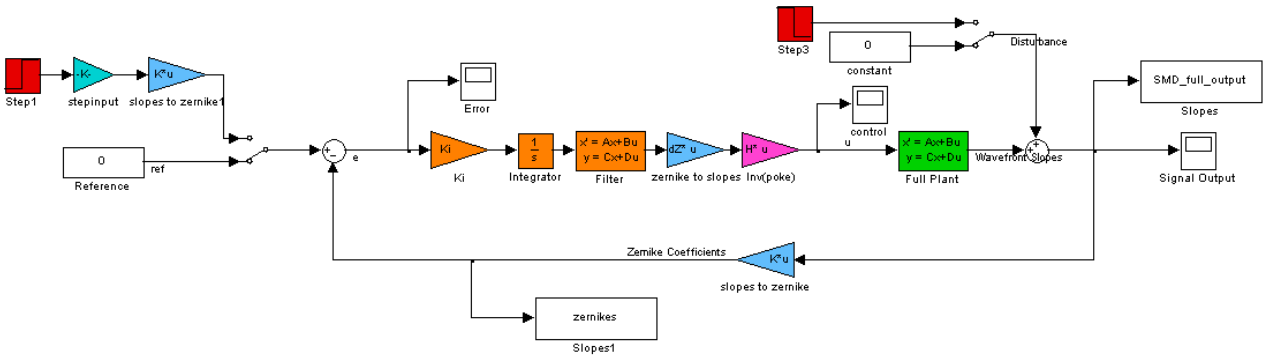

Figure 29. Zernike Control Model

The output of the plant is converted to the Zernike coefficients in the feedback loop by using the pseudoinverse of [dZ], then gained and integrated before being converted back to required sensor readings and finally using the inverse of the poke matrix transformed to actuator commands.

Each of the filters used in the SVD reduced model can also be used in the Zernike reduced model at the same frequencies, since the desire is to reduce natural frequencies in the physical system. Gains used in Zernike coefficient control cannot be compared directly to the gains used with pure classical control, since the Zernike control gain is on the Zernike coefficients and not on the error function, but the process for tuning gains and filters is the same as in pure integral control.

(1) No Filters. With no filters, the system is stable with a gain of 15 and a bandwidth of 2.4 Hz. The plot of the closed loop poles confirms the stability at this gain in Figure 30.

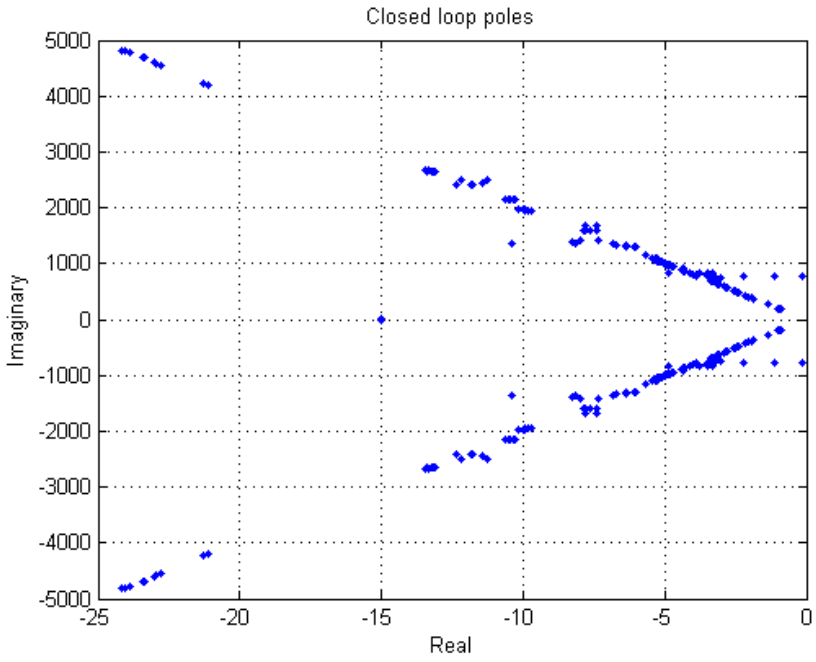

Figure 30. Zernike Control Closed Loop Poles, No Filters

As with the classic integral control, this does not meet the bandwidth requirements, but it is an improvement in bandwidth over the classic integral control alone. To achieve the required bandwidth of 10 Hz filters are needed to reduce the higher frequency resonances to allow the gain to be increased. The same filters that are used with the classic integral control are also used with the Zernike polynomial control.

(2) Notch Filters. The notch filter used for Zernike Integral control is shown in Figure 17. The max *Zernike gain* to achieve a stable system was 594, giving a bandwidth of 59 Hz, which is an 11% increase in bandwidth over the classic integral control method. The step response at this bandwidth is equivalent to the classic control method, as shown in Figure 31.

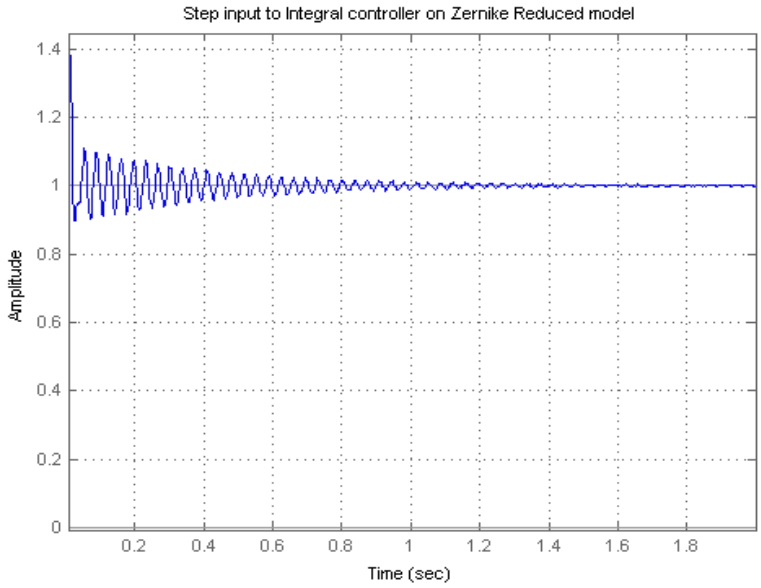

Figure 31. Step Response, Zernike Control, Notch Filter, Max Bandwidth

Simulations of the bounding case at minimum bandwidth, best performance, yield the results shown in Figure 32. The Zernike gain at this bandwidth is 46.

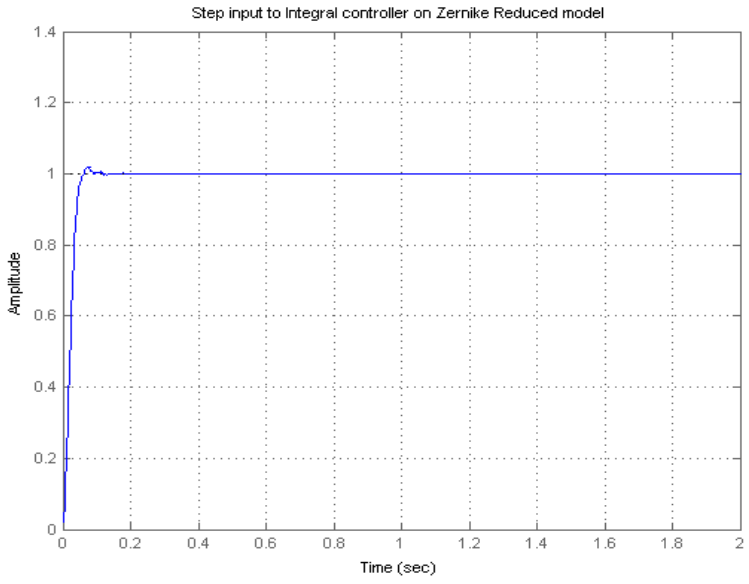

Figure 32. Zernike Control Step Response, Best Performance, Notch Filter

The performance at the lowest bandwidth is about the same, but the integrator is only controlling 21 channels, instead of 100 channels from the SVD reduced model.

(3) Elliptic Filter, 29 Hz Cut-off Frequency. The elliptic filter used for this analysis has is the same as used with the SVD-reduced classic control with the bode diagram shown in Figure 21. This elliptic filter produces the same results at the same bandwidth, 25.5 Hz, with the same gain of 113 as the 29 Hz Elliptic filter used in the classic control with SVD-reduced system. The plot of the step response for this system at the maximum bandwidth is shown in Figure 33.

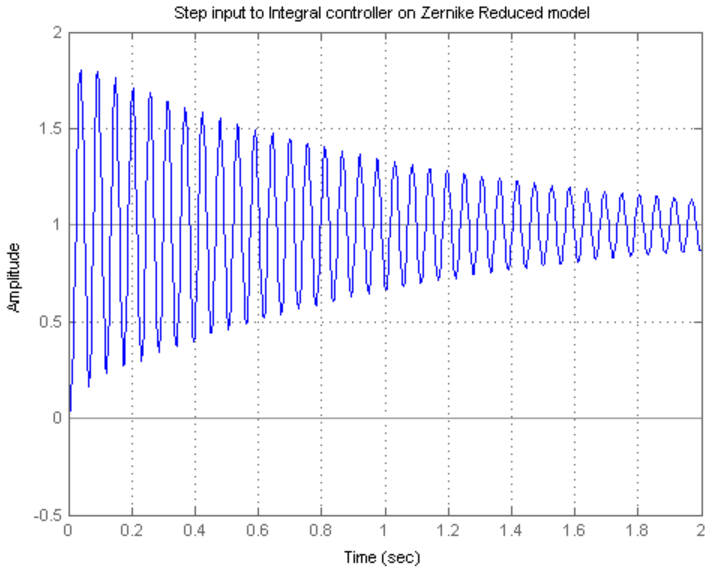

Figure 33. Step Response, Zernike Control, Elliptic Filter, 29 Hz, Max BW

Using the same gain tuning technique as before, the 29 Hz elliptic filter gain was tuned to 33 to achieve minimum bandwidth at 10 Hz. The results of the step response are shown in Figure 34.

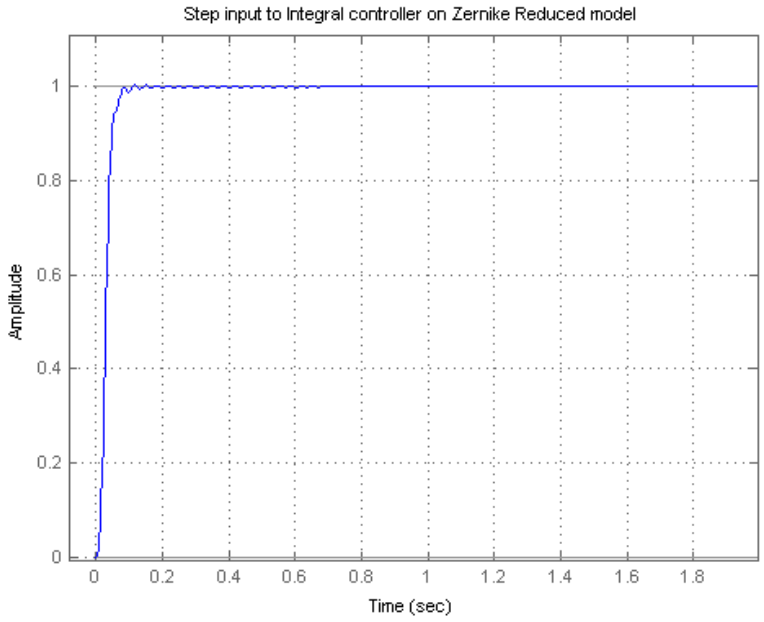

Figure 34. Step Response, Zernike Control, Elliptic Filter, 29 Hz, 10 Hz BW

(4) Elliptic Filter, 60 Hz Cut-off Frequency. The elliptic filter with a 60 Hz cut-off frequency used for Zernike control is also identical to the classical control filter with the same bode plot as Figure 24. The gains were tuned for a stable system with the best bandwidth achievable at 49 Hz using a gain of 201. The step response is shown in Figure 35.

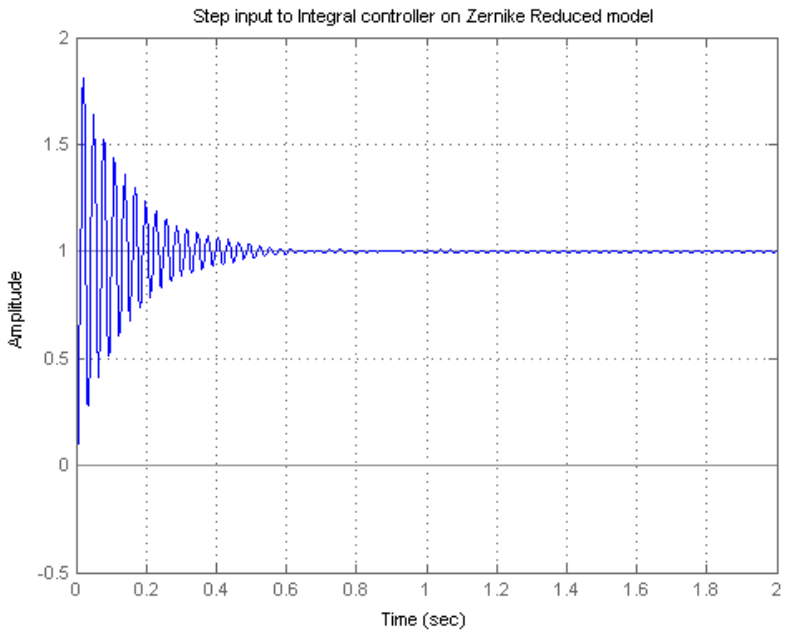

Figure 35. Step Response, Zernike Control, Elliptic Filter, 60 Hz, Max BW

The minimum required bandwidth of 10 Hz gain was 44, and the step response is shown in Figure 36.

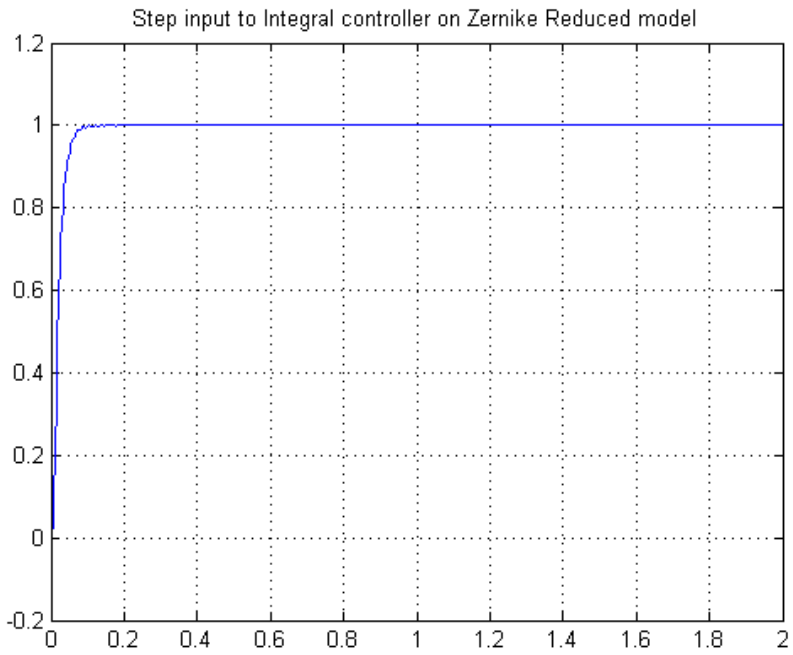

Figure 36. Step Response, Zernike Control, Elliptic Filter, 60 Hz, 10 Hz BW

B. ROBUST CONTROL

1. Introduction

The traditional classical control of adaptive optics relies on controlling the actuators by converting the sensor outputs to actuator inputs and ignoring the dynamics of the system. With the increase in complexity of the adaptive optics system by using large moving mirrors with more actuators, in order to achieve a high level of control, the dynamics of the system must be taken into account. In addition to the internal dynamics of the system, presence of noise and other factors cause problems with system stability. Classical control optimizes the performance of the system under ideal conditions and does not directly take into account the stability in the presence of uncertainty. Robust control optimizes the worst-case, or robust, performance instead of the best-case performance [10]. This is done by minimizing system norms.

2. Norms

A norm is a way of quantifying the size of a system mathematically. Although one could look at each of the individual elements of a vector, this would not give a good idea of the magnitude of the size of the system. The general formula for the vector *p-norm* is shown in Equation (4.10) [11].

$$\|x\|_p := \left(\sum_{i=1}^{n} |x_i|^p \right)^{1/p}, \text{ for } 1 \le p \le \infty \tag{4.10}$$

The 1-norm is the sum of all elements of x, the 2-norm is average size of a vector, and the infinity-norm is the maximum value of the vector, as shown in Equation (4.11).

$$\|x\|_\infty = \max_{1 \le i \le n} |x_i| \tag{4.11}$$

The concept of vector norms can also be applied to matrices as an induced matrix norm, which is said to be induced by a vector norm [11]. The general form of the induced matrix p-norm is shown in Equation (4.12).

$$\|A\|_p := \max_{x \ne 0} \frac{\|Ax\|_p}{\|x\|_p} \tag{4.12}$$

3. H_∞ and H_2 Norms

H_∞ and H_2 norms refer to the ∞- and 2- induced system norms in the Hilbert space. The Hilbert space is a space with a complete inner product with the norm induced by its inner product [11]. The utility of this space is that it extends the concept of the Euclidian plane to any number of dimensions, including all vector calculations mathematics. The Hardy spaces are a subset of the Hilbert spaces that include the H_∞ and H_2 induced norms. These norms are critical in developing robust control systems.

The H_2 norm of the G(s) system is defined in Equation (4.13).

$$\|G\|_2 = \sqrt{\frac{1}{2\pi} \int_{-\infty}^{\infty} \sum_i \sigma_i^2 (G(j\omega)) d\omega} \tag{4.13}$$

As previously discussed, the σ_i are the singular values of the system, which can be shown to be the squares of the natural frequencies. In a complex system, the σ values represent both direction and frequency, giving a magnitude to each of the singular values. Therefore, the H_2 norm represents the average magnitude of the average frequency of the system. By minimizing this norm, all singular values are pushed down over the average peak values. However, this is not an induced norm and does not follow the multiplicative property of norms in Equation (4.14).

$$\|AB\| \leq \|A\|\|B\| \tag{4.14}$$

The H_∞ norm in Equation (4.15) is an induced norm and follows the multiplicative property, therefore is more useful for analyzing the interconnections of systems. The $\bar{\sigma}$ is the largest singular value of the system.

$$\|G(s)\|_\infty = \max_\omega \bar{\sigma}(G(j\omega)) \tag{4.15}$$

By minimizing the H_∞ norm, the highest peak of the singular values is pushed down.

4. Loopshaping

Loopshaping is the process of determining the shape of the feedback loop. The “loopshape” specifically refers to the singular value plot of the open loop controller and plant model, as defined in Equation (4.16).

$$L = GK \tag{4.16}$$

Similar to designing a filter, it involves deciding what frequencies are in the performance range, and therefore should be increased in gain, and what frequencies are in the “robust” range, and should have a decreased gain. These frequencies and the foundation for building the robust controller are based on sensitivity functions.

a. Sensitivity Functions

The system used for reference when looking at the sensitivity functions and loopshaping is shown in Figure 37 where d_i is input disturbance and d is output disturbance and n is noise in the feedback loop.

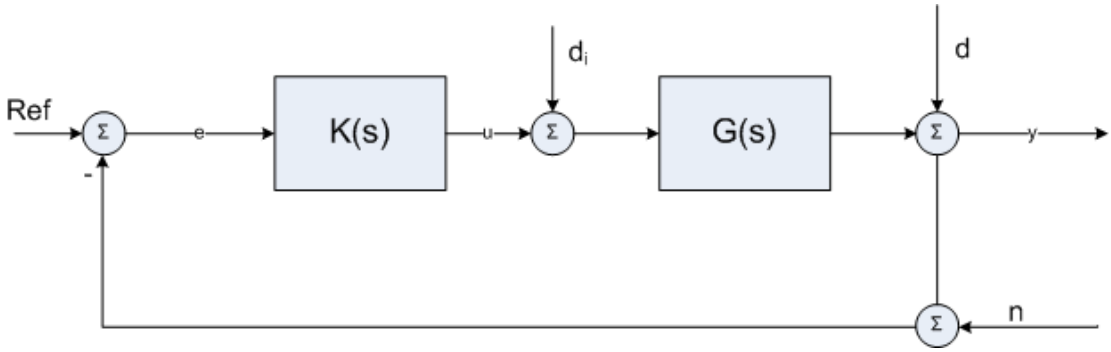

Figure 37. Control system with disturbances (after [11])

The output sensitivity function is defined by Equation (4.17).

$$S = (I + GK)^{-1} \tag{4.17}$$

This function quantifies how sensitive the control system is to disturbances at the output. There is also an input sensitivity matrix that relates the sensitivity of the input to disturbances, but the concern of this thesis is rejection of disturbances on the mirrors and other spacecraft noise, therefore the concentration is on the output sensitivities.

The complementary sensitivity function is defined in Equation (4.18).

$$T = GK(I + GK)^{-1} \tag{4.18}$$

The relationship between the sensitivity function and the complementary sensitivity function is shown in Equation (4.19).

$$T + S = I \tag{4.19}$$

From [11], if the closed-loop system is internally stable, it satisfies Equation (4.20).

$$y = T(ref - n) + SGd_i + Sd \tag{4.20}$$

The effects on the output by disturbance can be reduced by minimizing the output sensitivity function (S), but that of the noise (n) can be reduced by minimizing the complementary sensitivity function (T). In practice, this means that the maximum singular values of the sensitivity function over a range frequencies must be reduced, in order to reduce the effects of noise at those frequencies on the system. This is done by selecting weighting functions in order to specify the shape of the desired loop.

b. Weighting Functions

Weighting functions are chosen to increase the singular values of the system in the low frequencies and decrease the singular values in the higher frequencies. There are two weighing functions that are used for the H_∞ loopshaping for this thesis: W_1 and W_3. The W_1 weighting function is a weight added to the error and W_3 is a weight added to the measured output of the controller. The effect of adjusting W_1 is to adjust the inverse of the sensitivity function and increase performance in the lower frequencies, and having no affect at higher frequencies. The effect of adjusting W_3 is that it conditions the complementary transfer function, which has no effect on lower frequencies, but decreases the gain at higher frequencies. The overall effect gives a sigma plot as shown in Figure 38.

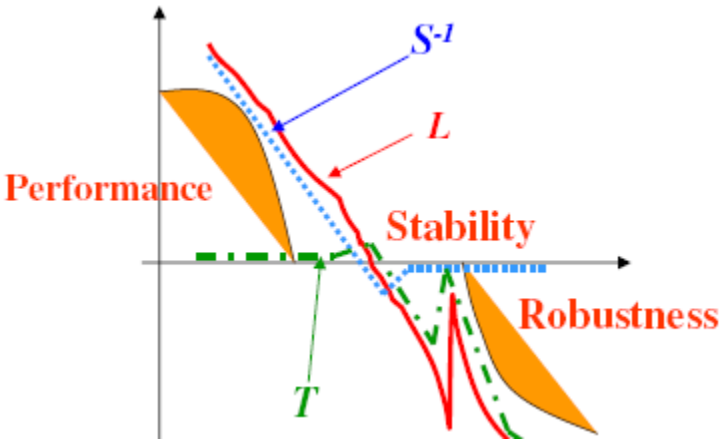

Figure 38. Robust Control Loopshaping (from [7])

The choice of weights for this thesis is based on the singular value plot of the G(s) plant, shown in Figure 39.

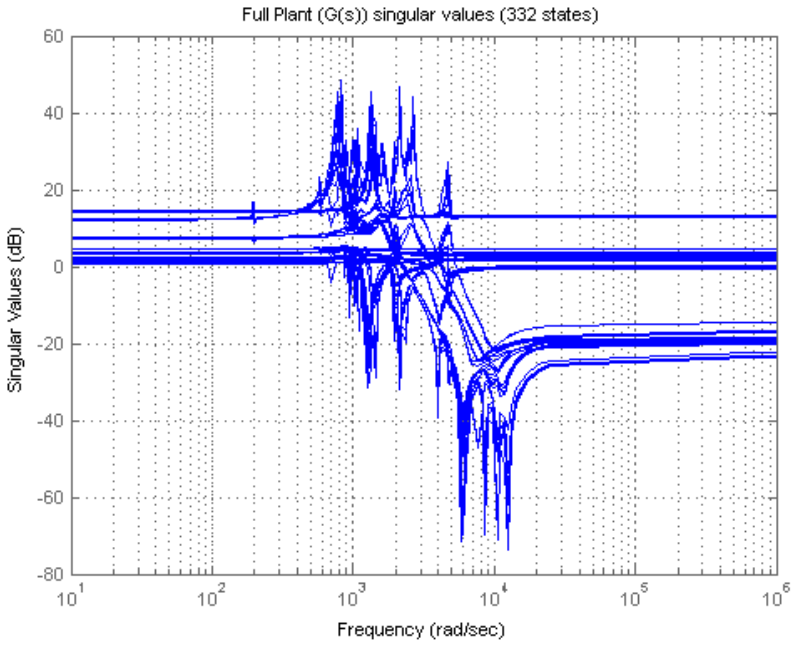

Figure 39. Plant Singular Values

The weighting functions designed for H_∞ control of the Segmented Mirror Telescope (SMT) are plotted in Figure 40.

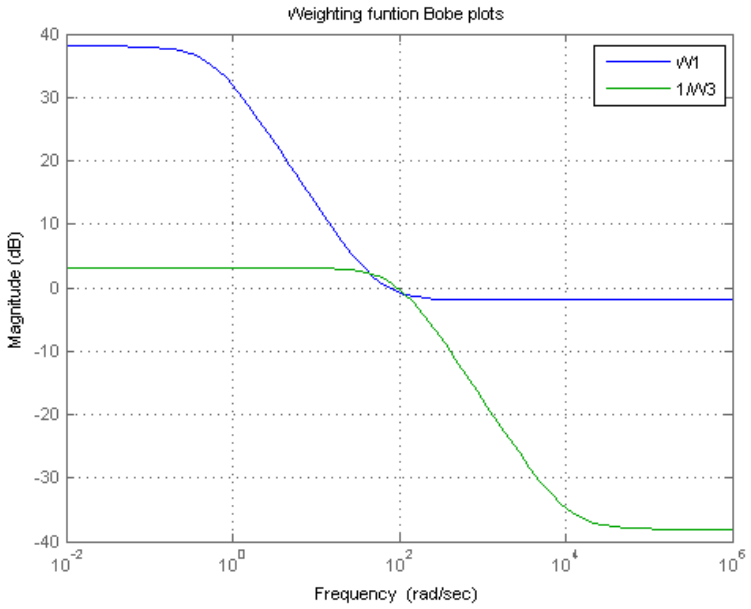

Figure 40. Weighing Functions for Robust Control of SMT

This choice of weighting functions drives down the higher frequencies for robustness and increases the gain at the lower frequencies to increase performance. The crossover frequency at 0 dB was chosen to be below the lowest natural frequency of concern for the system at 30 Hz.

c. H_∞ *Controller Synthesis*

Using the weighting functions previously described, the H_∞ controller is designed using a mixed sensitivity synthesis in Matlab. This function creates a controller transfer function that minimizes the H_∞ norm of the transfer function in Equation (4.21).

$$F_{y_1 u_1} \triangleq \begin{bmatrix} W_1 S \\ W_3 T \end{bmatrix} \tag{4.21}$$

This is the transfer function between the reference and the weighted functions of the augmented plant shown in Figure 41.

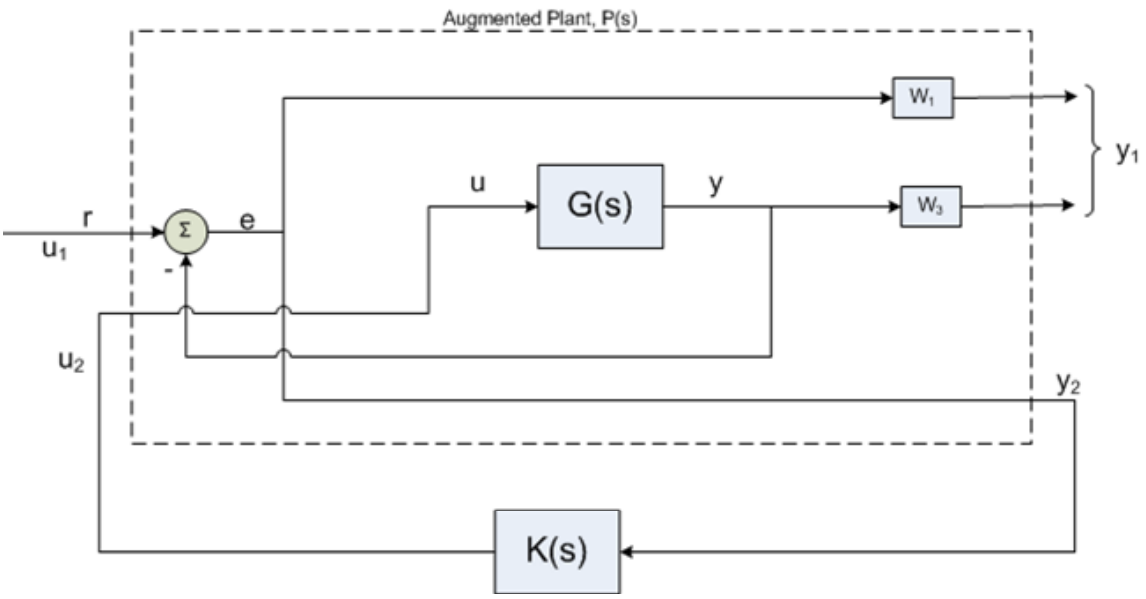

Figure 41. H_∞ Controller and Augmented Plant

Using the weighting functions from the previous section and the Segmented Mirror Telescope model with the mixsyn command in Matlab, the controller is synthesized. The loopshape, weighting functions, and sensitivity functions for the Segmented Mirror Telescope (SMT) are plotted in Figure 42.

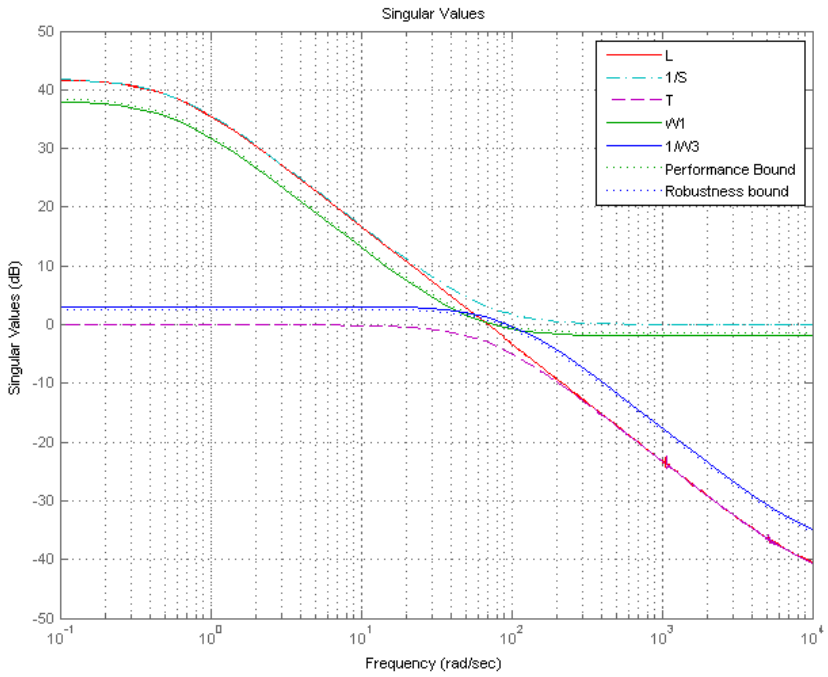

Figure 42. Loopshape of H_∞ Control System for SMT

The performance bound and robustness bound are calculated from Equations (4.22) and (4.23) respectively.

$$PerformanceBound = W_1 / \gamma \tag{4.22}$$

$$RobustnessBound = \gamma / W_3 \tag{4.23}$$

These calculations are based on the small gain theorem, which states that Equations (4.24) and (4.25) are true in order for a system to be robustly stable, referencing Figure 43 [11].

$$\|\Delta\|_\infty \leq 1/\gamma \text{ if and only if } \|M(s)\|_\infty < \gamma \tag{4.24}$$

$$\|\Delta\|_\infty < 1/\gamma \text{ if and only if } \|M(s)\|_\infty \leq \gamma \tag{4.25}$$

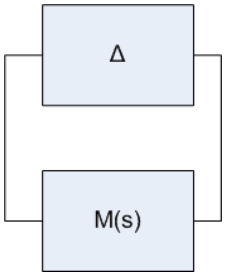

Figure 43. System With Uncertainty (after [11])

In Figure 43 and the small gain theorem, the Δ represents uncertainty in the model, M(s). The γ values used for the performance bounds are a product of the mixsyn command in Matlab when synthesizing the controller.

5. Model Uncertainty

The advantage of the robust controller is increased performance in the low frequency region, and robust performance in the higher frequency regions, and the ability to perform in the presence of uncertainties in the model on which the controller is based. The model was built based on the best knowledge of the actual system possible. However, as with any mathematical model, there are some assumptions that had to be made, therefore, there are uncertainties inherent in the model of the system. These uncertainties can be modeled as either additive or multiplicative, meaning they are either mathematically added to the model or multiplied into the model. The utility of creating an uncertain state-space model is that it can be used to test the ability of a certain controller to handle uncertainty, as well as perform robustness analysis on the controller.

Uncertainty can be either structured or unstructured. Unstructured uncertainty is added to the model as a percentage of error in the modeling. It is not physically possible to model it as a structured transfer function or other modeling technique. Structured uncertainty is error that can be modeled but is still present in the model, such as degradation of the parts of a system over time

changing the physical characteristics of the system or plant parameter variations [7]. The structured uncertainty can be modeled and added to the system.

The structured uncertainties are the concern of this thesis, therefore, they are multiplied into the SMT model in the A matrix, which has the structure shown in Equation (4.26).

$$A = \begin{bmatrix} [0] & [I] \\ \left[-\omega_n^2\right] & \left[-2\zeta\omega_n\right] \end{bmatrix} \tag{4.26}$$

The bottom left block of the A matrix contains primarily the natural frequencies and the bottom right term contains the damping of the system. For this thesis, 5% uncertainty was added to the natural frequencies and 10% uncertainty added to the damping due to modeling techniques having more error in the damping estimation.

C. COMBINED ROBUST AND CLASSICAL CONTROL

Robust control is useful for creating a control system that is able to perform and predict the performance of the controller in the presence of uncertainties in the plant model. Classical control is simple to understand and proven in real systems, but has to have the robustness to uncertainties built in by adjusting the gain and phase margins of the system, which reduce the performance of the system. By combining the high performance of the classical controller with the robust performance of the robust controller, a hybrid combined robust and classical controller can be designed.

It is important to note that this controller was built for regulation, which means that they are designed to drive the system output to zero. The stand-alone controllers are capable of controlling the slopes of the Shack-Hartmann Sensors to any desired value, which is what was done when tuning gains and filters for classical control, but the desired value of the Shack-Hartmann sensor will always be zero. Therefore, these controllers are truly regulators for the Segmented Mirror Telescope wavefront.

1. Parallel Combined Control

The classical and H_∞ controllers are combined in parallel as shown in Figure 44. The classical control elements are orange and the robust control elements are yellow. The filter used in this controller is the 60 Hz Elliptic filter with a gain of 45, which is the best performing filter of the classical control filters at the minimum 10 Hz bandwidth. The H_∞ controller used in this model is identical to the robust controller described in Section B of this chapter with a bandwidth of 10 Hz. It was designed as a stand-alone to control the plant without the classical controller.

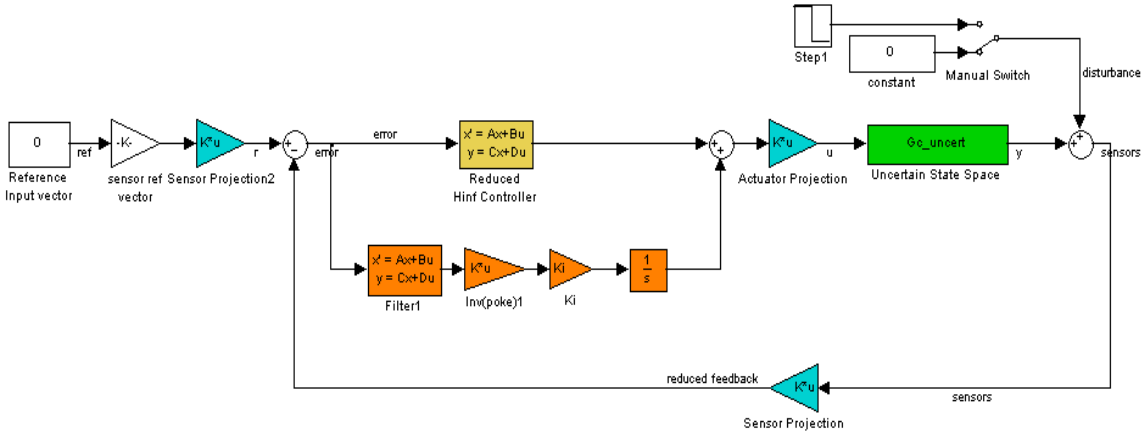

Figure 44. Parallel Combined Control Model

This controller is stable, as illustrated by the plot of the closed loop poles in Figure 45.

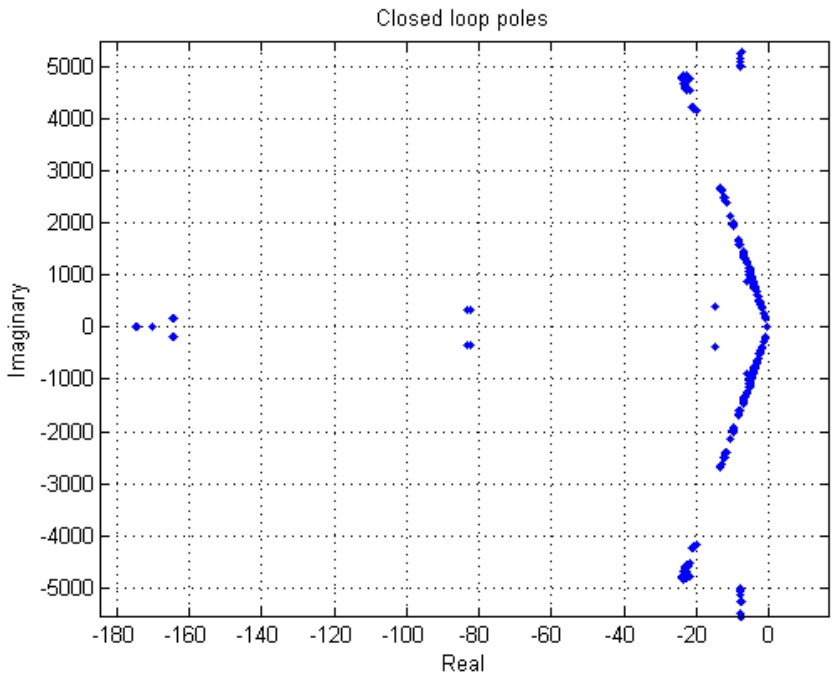

Figure 45. Parallel Combined Closed Loop Poles

The sigma value plot for the closed loop controller for this system is shown in Figure 46 and the bandwidth of the controller is 22.5 Hz.

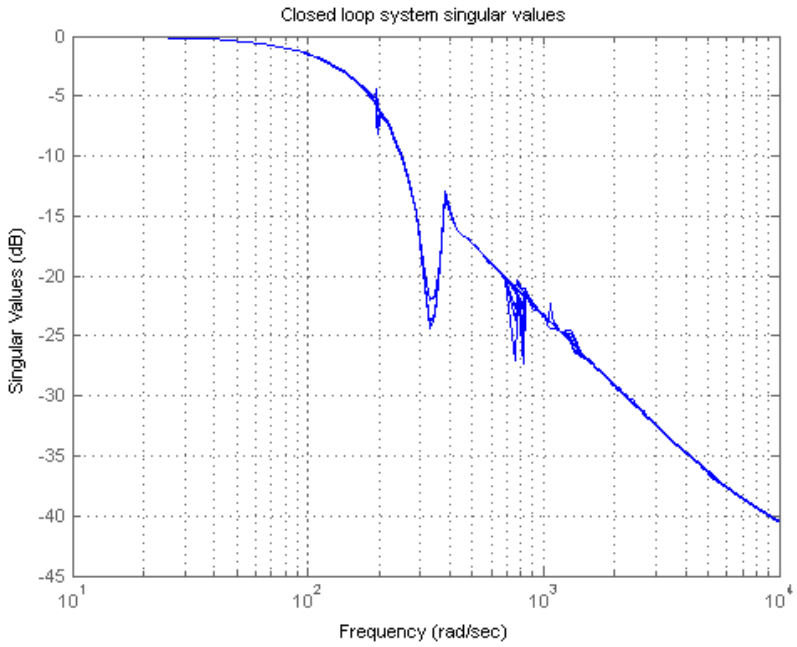

Figure 46. Parallel Combined Controller Closed Loop Singular Values

The advantage of this controller is that if something in the robust controller failed or something in the classical controller failed, the other controller can stand alone to control the system within bandwidth and performance specification.

THIS PAGE INTENTIONALLY LEFT BLANK

V. RESULTS AND ANALYSIS

A. PERFORMANCE AND COST MEASURES

To adequately compare the different control methods, meaningful cost and performance measures must be established and applied adequately. Typical control system performance measures include settling time, percent overshoot, and steady state error in response to a step input to the closed loop system. These factors will be used to compare the performance of the controllers in the closed loop system alone (input to output), but with a MIMO system, they must be applied slightly differently than with a SISO system.

Although the previously mentioned factors are good for comparison with a SISO system, they are not necessarily always good measures for MIMO systems since there are multiple signals that must be taken as a whole for evaluation of the performance. For the Segmented Mirror Telescope, the output of the system is the slopes of the wavefront. These slopes give a measure of error from zero of the wavefront when measured with respect to the root mean square (RMS) of the output slopes. This thesis uses the equation (5.1) to calculate the RMS values at each time step in order to get a graph of the surface error with respect to time, where x is the value of the slope and n is the number of Shack-Hartmann outputs.

$$RMS = \sqrt{\frac{\sum_{i=1}^{n} x_i^2}{n}} \tag{5.1}$$

RMS value graphs are easier to compare between the results of the control systems simulations without having to rely on judgment of how the actual slopes “look” when plotted. For every simulation, the RMS values are calculated based on the full wavefront, not the reduced system values.

Since the objective of SMT wavefront control is to maintain a flat wavefront in the presence of aberrations or external disturbances on the system, RMS is a good measure when a step input is imposed on the mirrors (through a

step function to the output of the simulation) and the response of the control system to the disturbance is observed. The step disturbance to all of the mirror segments consists of starting all Shack-Hartmann slopes at one, then after 0.001 seconds dropping the aberration to the mirrors to zero. Since the reference signal is zero, all of the slopes should go to zero. Settling time and steady state error can be compared between the different control systems based on the RMS of the sensor output using the disturbance as described. Part of the objective of this thesis include robustness of the model, therefore all simulations were done using the model containing uncertainties as discussed in Chapter IV.

The RMS values are a measure of the performance of the controller. Another type of cost measure is the size of the controller. Although these simulations were done on a computer with nearly "unlimited" resources, the size of the control system is somewhat irrelevant. However, when the control system is instantiated as an actual control system for a satellite, it will become important to keep the size down for power, complexity, and memory use purposes. Therefore, a way of determining the "size" of the control effort is necessary as a cost measure. A good way of measuring the size of the control system is by determining the order of the control system. The order of a state-space model is simply the number of states in the model. For an integrator in the integral control system, the order is the number of channels being integrated within the specific control systems. Therefore, each of the control systems will be evaluated for size of the control system by order of the controller. For example: the Zernike elliptic filter is a 6^{th} order filter multiplied by 21 channels used for control plus 21 channels of integration gives a control size of 147.

The size and bandwidth of all of the different control techniques used in this thesis are shown for comparison in Table 3. These numbers are based on the sizes of the reduced systems specifically chosen for this thesis, but give a basis for comparison of the types of control techniques.

Table 3. Cost Comparison of Control Methods

Controller	**Size**	**Max Bandwidth**
Classic Control, Notch	500	53 Hz
Classic Control, Elliptic 29 Hz	700	25 Hz
Classic Control, Elliptic 60 Hz	700	44 Hz
Zernike Control, Notch	105	59 Hz
Zernike Control, Elliptic 29 Hz	147	25.5 Hz
Zernike Control, Elliptic 60 Hz	147	49 Hz
Robust Control	282	10 Hz*
Parallel Combined Control	429	22.5 Hz*
*Note: The Robust controller and the H_∞ controller for the Parallel Combined Controller were designed for 10 Hz. This bandwidth is not necessarily representative of the Max bandwidth of the robust controller. The Parallel combined controller could also be designed to 10 Hz bandwidth, if desired.		

B. RESULTS

1. Classical Control

All of the classical integral controllers are evaluated at the best performance condition, which equates to minimum bandwidth at 10 Hz. The following figures show the response in simulation of the sensor outputs starting at a value of one and regulated to zero by the control system.

a. Notch Filter

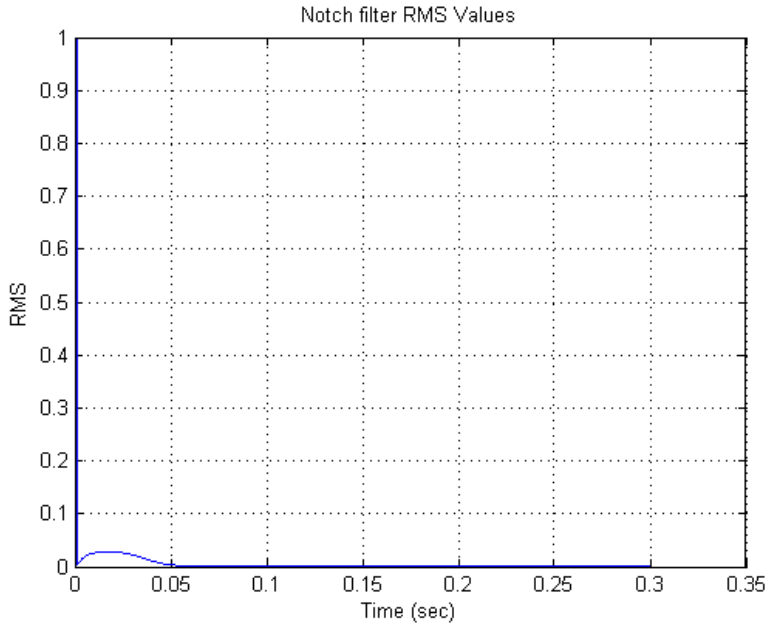

Figure 47. Classical Control, Notch Filter RMS

b. Elliptic Filter, 29 Hz Cut-off Frequency

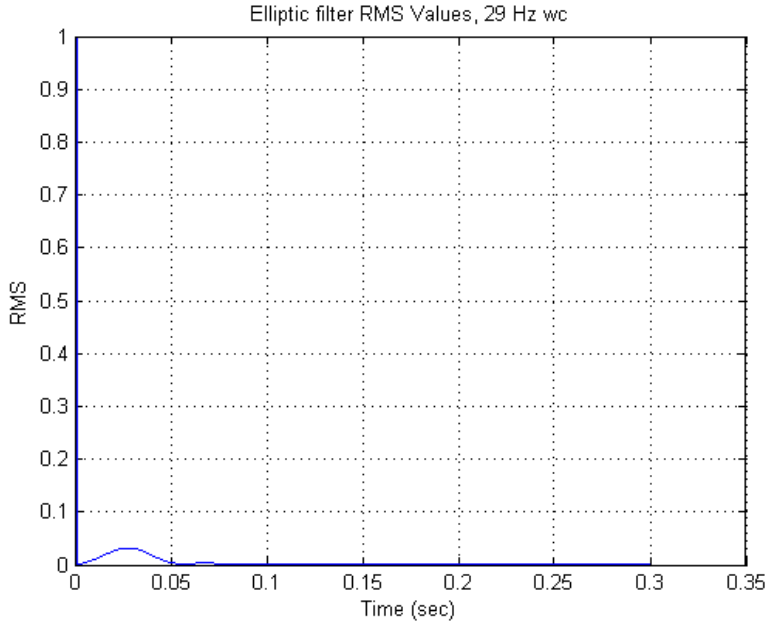

Figure 48. Classical Control, Elliptic Filter, 29 Hz Cut-Off RMS

c. Elliptic Filter, 60 Hz Cut-off Frequency

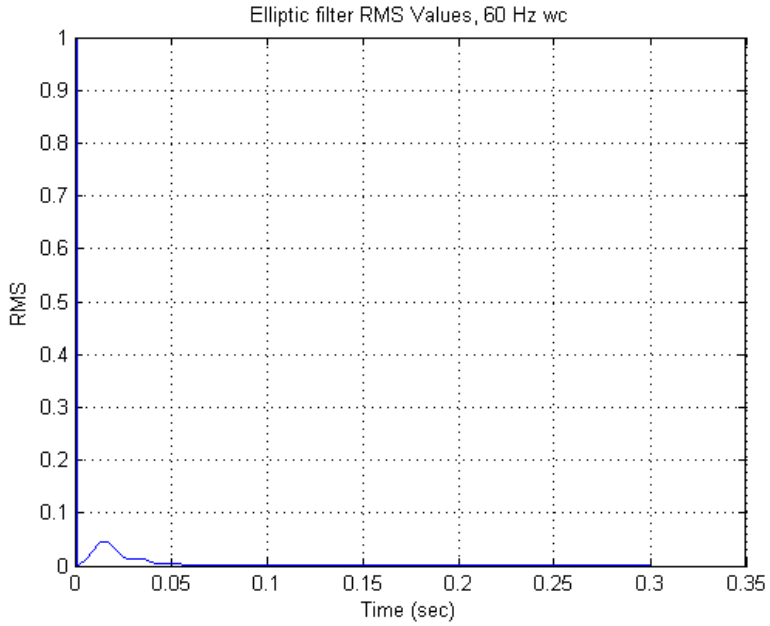

Figure 49. Classical Control, Elliptic Filter, 60 Hz Cut-Off RMS

d. Zernike Control, Notch Filter

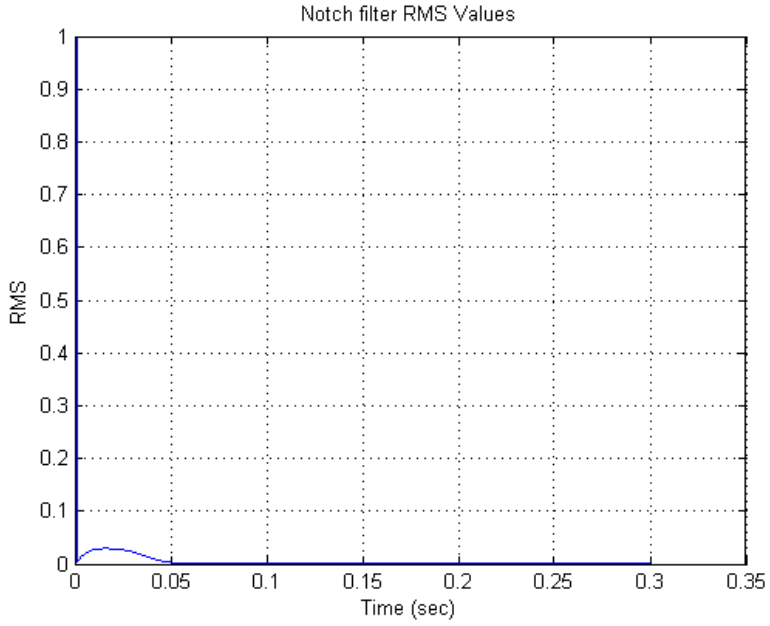

Figure 50. Zernike Control, Notch Filter RMS

e. Zernike Control, Elliptic Filter, 29 Hz Cut-off Frequency

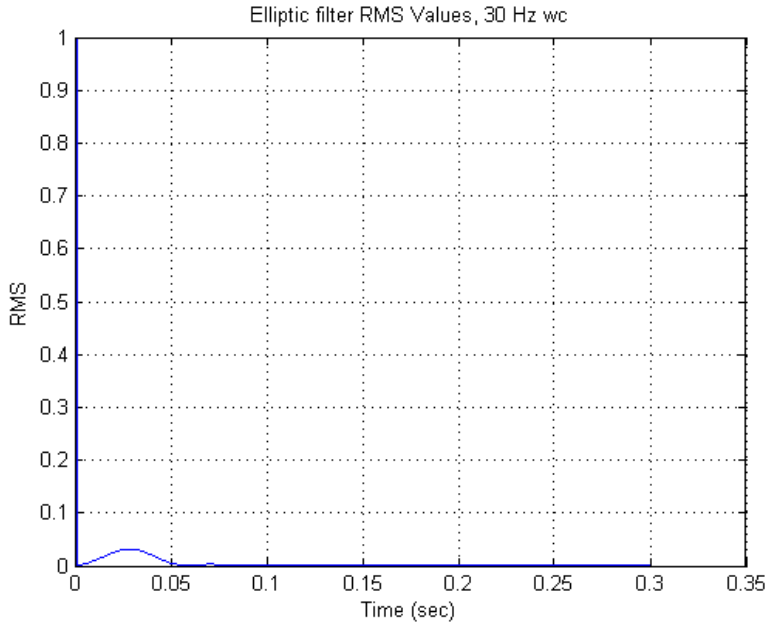

Figure 51. Zernike Control, Elliptic Filter, 29 Hz Cut-off RMS

f. Zernike Control, Elliptic Filter, 60 Hz Cut-off Frequency

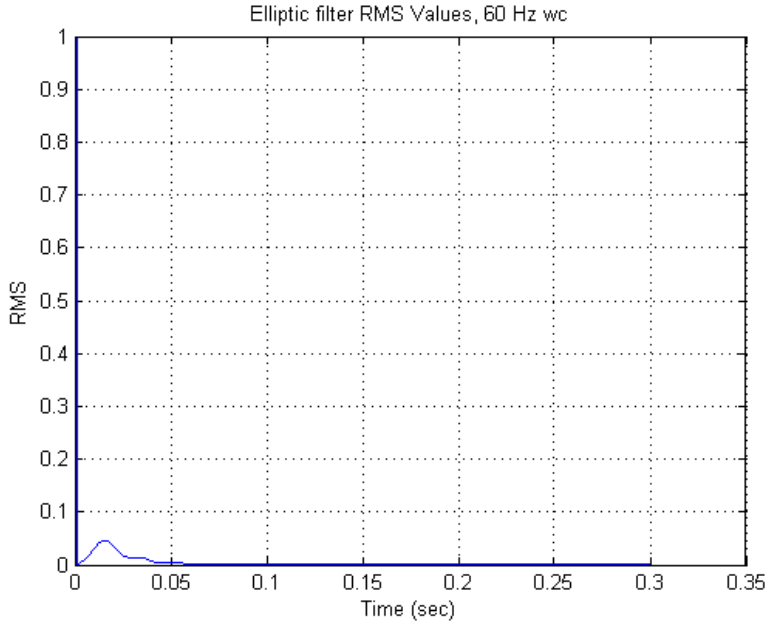

Figure 52. Zernike Control, Elliptic Filter, 60 Hz Cut-off RMS

2. Robust Control

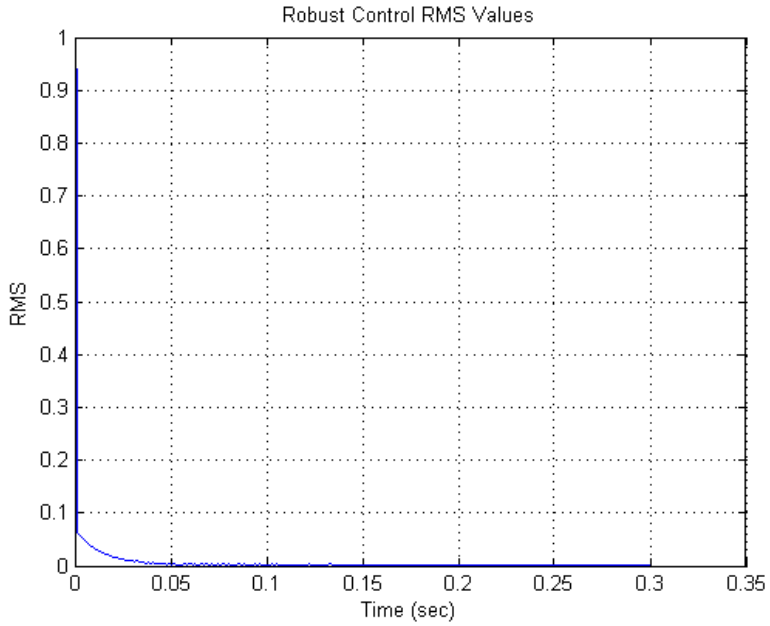

Figure 53. Robust Control RMS

3. Combined Robust And Classical Control

a. Parallel Combined Control

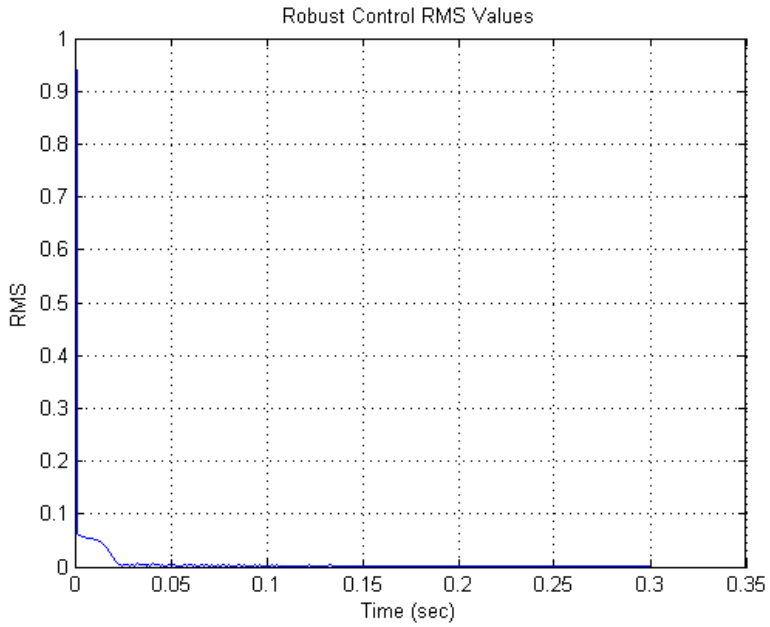

Figure 54. Parallel Combined Control RMS

C. RESULTS AND COST ANALYSIS

To compare the different control methods by performance, RMS plots for one classical control, robust control, parallel combined control, and series combined control are shown for the first 0.08 seconds in Figure 55. Although all of the classical control methods were similar, the elliptic filter with 60 Hz cut-off frequency was chosen since it had the best performance.

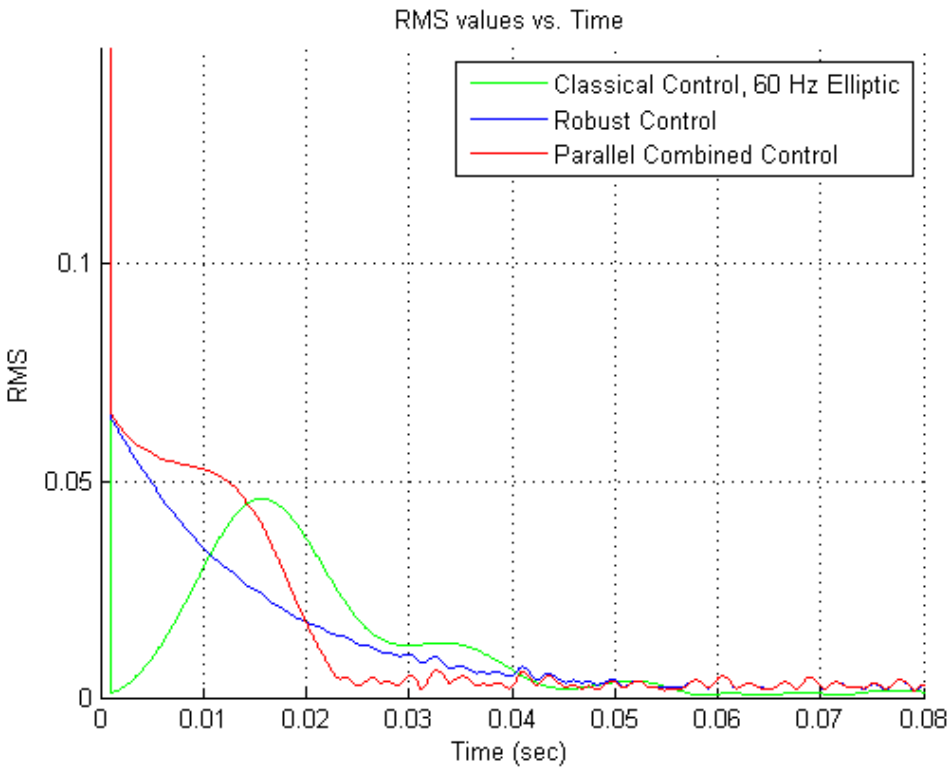

Figure 55. RMS Values Comparison

Looking at Figure 55, the parallel combined controller appears to have the fastest settling time, reaching steady state at 0.022 seconds, while the robust controller and classical controller reach steady state at 0.05 and 0.058 seconds respectively. Notice, however, that both of the controllers that have a robust controller eventually have a steady state error, while the classical controller at steady state has a noticeably smaller steady state error. Eventually, the robust controllers would have reached a zero steady state error, but the classical controller seems to reach zero steady state faster. This error might be insignificant, since the RMS values at this point are most likely in the system noise, which was not included in the analysis.

From the cost-to-benefit viewpoint, the Zernike controller with the Notch filter has the smallest size at 105. Given that it has comparable control to the other filters and the best possible bandwidth, it is the best of the classical control

methods from a size-performance comparison, as well as the best controller over-all for size-performance. The robust controller has better performance as far as settling time, but the cost at over double the Zernike notch controller at 282 does not seem to outweigh the increase in settling time. From a pure performance standpoint, the parallel combined controller has the best performance with twice the bandwidth of the classical and robust control methods alone. The trade-off is the greater than quadruple size of the combined controller, which is a system design consideration for the Segmented Mirror Telescope.

VI. SUMMARY AND FUTURE WORK

A. SUMMARY

The future of space telescopes is the movement from primary optics that are large and monolithic to much larger, lightweight, segmented mirrors. With this increase in size and decrease in mass comes an increase in flexible modes and natural frequencies that must be controlled. These mirrors are highly susceptible to onboard aberrations from other sources of noise, as well as external distortion of the light entering the mirrors. There are several techniques available to the control system engineer to control the mirrors to create a flat wavefront. The control systems presented in this thesis include robust control, classical control, and a hybrid combination of robust and classical control.

The work on this thesis is specific to the Segmented Mirror Telescope, which has six hexagonal mirror segments with the facesheet controlled by 936 actuators and the slopes of the wavefront measured by 732 Shack-Hartman sensor outputs. The size of a controller for the entire system would be extremely large; therefore, it is necessary to reduce the system for generation of a control law that can be analyzed using Matlab and Simulink. Model input/output reduction was done using two different methods, Singular Value Decomposition and Zernike Polynomial Coefficients. The Singular Value Decomposition technique is used to determine the most influential singular values, then truncate the influence matrices and apply the resulting transformation matrices to the input and the output of the system. This allowed an H_∞ controller to be generated based on a reduced model and allowed for tuning of the filter frequencies and gains. The other method of reducing the inputs and outputs to the system utilized Zernike Polynomial Coefficients, relating the different wavefront shapes to the slope outputs of the Shack-Hartmann sensor.

The classical control method consisted of an integrator, a gain, and a filter for each of the reduced system channels. By tuning the gains and filter

frequencies, a stable system with both a minimum and maximum bandwidth could be achieved for three different cases of filters: a notch filter, an elliptic filter with 29 Hz cut-off frequency, and an elliptic filter with 60 Hz cut-off frequency. Each of these filters are applied to the SVD-reduced and Zernike coefficient-reduced systems. The SVD-reduced system was reduced to 100 channels and the Zernike coefficient-reduced system was reduced to 21 channels. The results were all very close and could not be distinguished between the two reduction techniques. The cost analysis shows that all of the Zernike coefficient-reduced controllers were much smaller than the SVD-reduced systems, and given that they produce the same results, if a classical controller is desired, the Zernike-reduced method is superior in cost-to-benefit. The performance of the classical controller was always measured at the minimum bandwidth of 10 Hz. The trade-off with the classical controller is that with increased bandwidth comes decreased performance.

The H_∞ controller provided increased performance over the classical controller techniques. Since it is twice the size of the Zernike coefficient-reduced controller and half the size of the SVD-reduced controller, it falls in the middle for cost-benefit analysis. The benefit of this controller is hampered by the complexity, though. One of the factors that could not be tested with this thesis is the robustness of the controllers. If there is an area that the robust controller would be better, it is in resistance to aberrations on the mirrors.

The H_∞ controller and the classical controller are combined in parallel for this thesis. For the parallel combined controller, the performance was increased over each of the controllers alone and the bandwidth at this performance was doubled. This makes the parallel combined controller superior in performance over all other methods. This performance comes at a cost, though, at quadruple the size of the best performing classical controller.

B. FUTURE WORK

One of the areas that future work can be done on this thesis is experimenting with the number of Zernike polynomials used for the reduced controller. When looking at the direct readout of the Zernike polynomials from the simulations, the first two are by far the most influential and the rest of them are very small. The size of the controller used for Zernike control could be decreased significantly by decreasing the number of coefficients used. The benefit of this would have to be weighed with the assumed decrease in performance of the resulting reduced system.

While conducting research for this thesis, the integral controller was also connected in series with the robust controller. The series combined controller showed promise in analysis of the reduced system; however, it failed to perform in the full system test. More research must be done on different methods of creating the series-connected combined controller. Future work with the series combined controller should also include applying it to a full system rather than a reduced one to look at the performance.

The parallel combined controller had an H_∞ controller that was based on 10 Hz bandwidth, but when combined with the classical controller, the bandwidth doubled. Future work on the parallel combined controller would be to design the two controllers to have a combined bandwidth of 10 Hz. This would most likely result in a better performing system at the specified bandwidth.

The reduction of these systems for control were based on perceived number of necessary singular values or Zernike polynomials, and consequently the costs and conclusions were based on these chosen values. As a follow-on different numbers of Zernike polynomials and singular values should be chosen and the results compared to give a better comparison of cost-vs-performance.

All of these methods should eventually be applied to a real system. Although they performed well in simulation using Matlab and Simulink, they might behave differently in an actual testbed. The most obvious testbed is the Segmented Mirror Telescope demonstrator.

LIST OF REFERENCES

[1] R. C. Olsen, *Remote Sensing from Air and Space*. Bellingham: The Society of Photo-Optical Instrumentation Engineers, 2007.

[2] National Aeronautics and Space Administration. (2009, Oct.) Hubble Space Telescope. [Online]. http://hubble.nasa.gov/index.php

[3] D. C. Redding, et al., "Wavefront Sensing and Control for Large Space Optics," vol. 4, no. 1729, 2003.

[4] J. Z. Lou, D. Redding, N. Sigrist, Y. Zhang, and S. Basinger, "JWST On-Orbit Multi-Field Wavefront Control with a Kalman Filter," vol. 5867, no. 58670T, 2005.

[5] R. K. Tyson, *Introduction to Adaptive Optics*. Bellingham: SPIE-The International Society for Optical Engineering, 2000.

[6] J. C. Wyant. (2003) Zernike Polynomials for the Web. [Online]. http://www.optics.arizona.edu/jcwyant/Zernikes/ZernikePolynomialsForTheWeb.pdf

[7] D. C. Burtz, "Fine Surface Control of Flexible Space Mirrors Using Adaptive Optics and Robust Control," Dissertation, 2009.

[8] M. R. Allen, "Wavefront Control for Space Telescope Applications Using Adaptive Optics," Masters Thesis, Naval Postgraduate School, Monterey, 2007.

[9] W. H. Southwell, "Wave-front estimation from wave-front slope measurements," *Journal of the Optical Society of America*, vol. 70, no. 8, pp. 998-1006, Aug. 1980.

[10] B. W. Frazier, R. K. Tyson, J. Ackman, and M. Smith, "Closed loop results of a compact high-speed adaptive optics system with H-inf control," *SPIE*, vol. 5169, pp. 37–42, 2003.

[11] K. Zhou and J. C. Doyle, *Essentials of Robust Control*. Upper Saddle River, United States of America: Prentice-Hall, Inc., 1998.

[12] N. S. Nise, *Control Systems Engineering*, 4th ed., B. Zobrist, Ed. Pomonoa, United States of America: John Wiley & Sons, Inc., 2004.

THIS PAGE INTENTIONALLY LEFT BLANK

INITIAL DISTRIBUTION LIST

1. Defense Technical Information Center
   Ft. Belvoir, Virginia

2. Dudley Knox Library
   Naval Postgraduate School
   Monterey, California

3. Dr. Brij Agrawal
   Naval Postgraduate School
   Monterey, California

4. Dr. Jae Jun Kim
   Naval Postgraduate School
   Monterey, California